UNIVERSITY OF CALIFORNIA SAN DIEGO

Position Localization for Interventional Pain Management Therapies

A thesis submitted in partial satisfaction of the requirements for a degree of

Master of Science in Bioengineering

by

Bryan Nguyen

Committee in charge:

Professor Frank E. Talke, Chair
Professor Gert Cauwenberghs, Co-Chair
Professor Bruce C. Wheeler

2022

The Thesis of Bryan Nguyen is approved, and it is acceptable in quality and form for publication on microfilm and electronically.

University of California San Diego

2022

TABLE OF CONTENTS

LIST OF FIGURES

LIST OF APPENDIX FIGURES

LIST OF TABLES

ACKNOWLEDGMENTS

I would like to thank Professor Frank Talke for his support and guidance throughout my project. He has been significant in helping me enjoy my work and gain the confidence to believe in my research.

I would like to thank Dr. Farshad Ahadian, for helping me learn much more about pain management therapies and allowing me the opportunities to shadow him. For every question I asked, he would often answer an additional ten different questions. His support and guidance were critical to the development of this project.

I am very grateful to Matthew Kohanfars, who welcomed me into the Talke Lab, gave me extensive advice, and answered all of my questions. He was fundamental in helping me set a strong foundation and a clear plan for the whole project.

I would also like to thank Dr. Gert Cauwenberghs for his support as the co-advisor of my project. Whenever I talked to him about my research, he listened carefully and gave very insightful feedback along with Akshay Paul, a Ph.D student in his lab.

I would like to thank Mitsuhiro Jo-Zee and Darin Tsui for their assistance on the project. They joined the project to work on the marker materials and tracking and I believe that the project will be successful and grow under them and the two new members of this project, Brandon Lee and Kaitlyn Strandberg.

Thank you to the Talke Lab for their immense support and friendship. Whenever I had a question or needed help, they would happily listen and try their best to assist me. They also helped make the lab a great work environment and a place where I was always comfortable and happy. Thank you Dr. Karcher Morris, Rafaela Simoes-torigoe, Po-han Chen, Brian Li, and everyone else in the Talke Lab.

I would like to thank my friends, Daibo Zhang and Irene Lee for helping me with statistics and proofreading my thesis. Lastly, I would like to thank all of my friends and family for their support and encouragement throughout the whole year.

ABSTRACT OF THE THESIS

Position Localization for Interventional Pain Management Therapies

By

Bryan Nguyen

Master of Science in Bioengineering

University of California San Diego, 2022

Professor Frank E. Talke, Chair

Professor Gert Cauwenberghs, Co-Chair

Back pain is one of the leading causes of disability in the world. Interventional pain management therapies often include epidural steroid injections or radiofrequency ablations to alleviate back pain. However, current techniques use fluoroscopy, which exposes both the patient and physician to radiation and require an experienced physician to accurately translate the 2D x-ray images to a 3D mental image. An augmented reality navigation system is proposed as a solution to eliminate radiation exposure and offer a low-cost method to overlay a 3D MRI model of the patient's anatomy on top of the patient to increase the speed and safety of spinal surgical procedures. Non-invasive skin markers with ArUco codes will be used to register the MRI model on top of the patient's body during the procedure. Experiments involving an XYZ platform were run to determine the tracking accuracy of the ArUco codes and which variables potentially present in an operating room could affect that tracking accuracy. It was determined that the ArUco codes had submillimeter error, thus showing their feasibility in pain management navigation systems.

Chapter 1 Back Pain and Management

1.1 Back Pain

Back pain is the leading cause of non-fatal health loss and disability globally – in 2017, there were approximately 577 million people with back pain [1]. It is especially prevalent in women and those who are 40 years or older [2].

There are many potential causes of back pain; from obesity and lack of exercise to aging or genetics, it can even be caused by psychological disorders such as stress, anxiety, and depression [2–8]. Whatever the cause, back pain has many debilitating effects on its victims and can lead to loss of physical activity, inability to perform job functions, heavy financial burden, relationship strain, and more [9]. In addition to individuals, back pain can have a heavy impact on the economy. An analysis of the Medical Expenditure Panel Survey (MEPS) from 1997 to 2005 found that back and neck problems cost a total of $86 billion in the United States that year, a 65% increase in health expenditures from 1997 to 2005 [10].

With the advancement of healthcare and technology, the average lifespan of people around the world has greatly increased. As society sees people reach older ages than ever before, it is likely that the population of people with back pain will also increase [1]. Given the widespread prevalence of back pain and its debilitating effects on everyday activities, it is important to proactively address back pain now before it becomes a bigger burden in the future.

1.2 Current Back Pain Treatments

Back pain is classified from grades I to IV, where grade I is the least painful and grade IV is the most severe [2]. To match the large range in back pain severity, there exist many different treatment options.

For nonspecific back pain, physical therapy is often recommended as well as accompanying activities such as exercise, yoga, and massages before exploring other treatments [11–13]. These options are the least invasive treatments and are usually done for several months at a time with periodic evaluations by a physician to assess whether improvement is being seen. Physical therapy is the first step in treatment for all levels of back pain severity, not just patients with less severe cases, because it is non-invasive. If physical therapy does not alleviate the back pain, then pharmacological therapies such as nonsteroidal anti-inflammatory drugs, muscle relaxants, narcotics, or pain relievers may be used [14,15].

For the most severe back pain and problems, patients may undergo spinal surgery of which three different options exist: spinal decompression, spinal fusion, and disc arthroplasty [16–19]. Spinal decompression surgery is usually chosen when parts of the spine impinge on nerves and involves the partial or complete removal of those structures. Spinal fusion is used to stop excessive movement of an unstable vertebral segment by fusing adjacent vertebrae with bone graft (autograft or allograft) and surgical hardware [19]. Lastly, disc arthroplasty is used to replace a dysfunctional intervertebral disc with an artificial disc [19,20]. Spinal surgery is generally recommended as a last resort only when less drastic treatments fail to alleviate back pain over a prolonged period.

Interventional Pain Management Therapies

In cases where physical therapies and medications are not effective but the back pain is not severe enough to warrant surgery or the patient refuses to undergo surgery, interventional pain management therapies are often suggested. Two common interventional pain management therapies performed are epidural steroid injections and radiofrequency ablations.

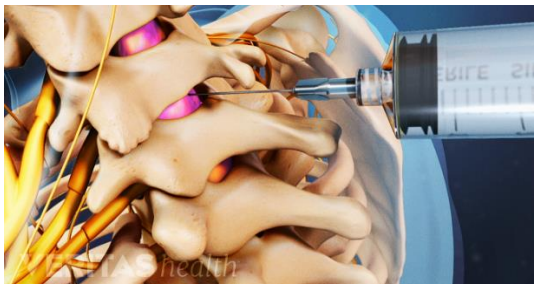

Figure 1: Epidural steroid injection procedure [21]

Epidural steroid injections (ESI) are the targeted delivery of corticosteroids near inflamed nerve roots to numb pain and reduce inflammation. Once the corticosteroids reach the surrounding cells, they are transported into cell nuclei and upregulate anti-inflammatory proteins while also downregulating inflammatory proteins [22]. To reach the nerves and inflamed surrounding area, the steroids are injected into the epidural space, which is located in between the vertebral canal and spinal cord and is filled with cerebrospinal fluid. The epidural space can range from 1 mm to 5 mm in depth from the cervical to lumbar spine respectively [23]. ESIs are not meant to cure back pain but instead provide pain relief for around three to six months, allowing patients to focus on their original rehabilitation program [24,25].

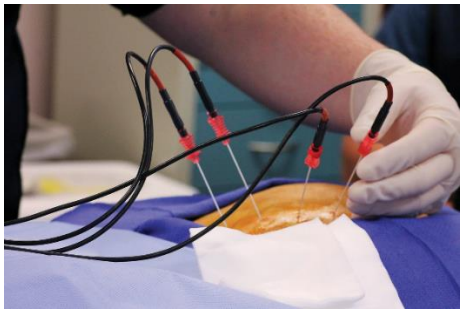

Figure 2: Radiofrequency ablation procedure [26]

Radiofrequency ablations (RFA) are the use of electrical energy with an insulated needle and thermocouple to provide a controlled temperature lesion of the desired nerves. The tip of the needle is usually set to around 80 to 90℃ and the size of the lesion varies depending on the temperature, tip diameter and length, tissue properties, and nearby vasculature [27]. RFA treatments can last anywhere from two months to three years depending on nerve regeneration and whether the pain returns or not [28]. RFAs have an immediate effect due to the ablation of nerves and have a longer duration of effect compared to ESIs.

1.3 State of the Art Technologies

1.3.1 Virtual, Augmented, Mixed Reality

Many of the current state of the art technologies utilize virtual, augmented, or mixed reality to help physicians and surgeons to better visualize inside the patient's body. This is especially helpful in modern procedures, especially minimally invasive surgeries [29].

Virtual reality (VR) is a procedure where the real-life surroundings are replaced by a completely virtual environment through the use of a headset [30]. VR has been established as a learning and training tool for surgeons to use without the need of a cadaver or the risk of operating on a live patient [31]. However, since virtual reality separates the user from real life, it is limited to being a training tool for surgeries.

Augmented reality (AR) overlays a digital layer on top of the real-life environment to give a person additional information about things around them. Augmented reality has been used in a wide variety of procedures including neurosurgery, otolaryngology, and maxillofacial surgery [32,33]. Studies have shown that the use of augmented reality has similar accuracy compared to conventional methods such as fluoroscopy and ultrasound [33–35]. It is especially helpful for novice surgeons to learn how to perform procedures quickly and safely [34,36].

Mixed reality (MR) attempts to combine the features of both virtual and augmented reality by allowing users to interact with both the real and virtual world. Compared to virtual and augmented reality, mixed reality is not as well-known and the distinction between mixed and augmented reality is not always clear [30]. A difference between them is that mixed reality enables users to see depth and perception of the virtual objects as they move around and view those objects. Tianjin University and the Sun Yat-sen University Cancer Center had a successful study using mixed reality with brachytherapy, where the surgeon used a virtual menu to interact with virtual models and images [37].

The goal of virtual, augmented, and mixed reality in surgeries is to help provide surgeons the extra training or input during a procedure they need to increase surgical accuracy and decrease the procedure time.

1.3.2 Current Systems

There have been many computer navigation and robot-assisted navigation systems developed in recent years for spine surgeries (Table 1).

Table 1: A List of Some of the Current Navigation Systems Used in Spine Surgery [38].

Technologies for spinal navigation

Product	Vendor
StealthStation	Medtronic
Intraop spinal navigation	Brainlab
Machine-vision image-guided surgery system	7D Surgical
Stryker NAV3i	Stryker
Ziehm Vision (FD) Vario 3D	Ziehm
Mazor X Stealth robot	Medtronic
ExcelsiusGPS robot	Globus
ROSA ONE Spine robot	Zimmer Biomet
TIANJI robot	Tinavi
xvision AR system	Augmedics
Arcadis Orbic 3D	Siemens
Pulse navigation	NuVasive

Although these systems were developed for use in spine surgeries, there are many technologies, such as Augmedics xvision, Phillips ClarifEye, and SeaSpine 7D Surgical, that can be translated to interventional pain therapies.

Augmedics xvision

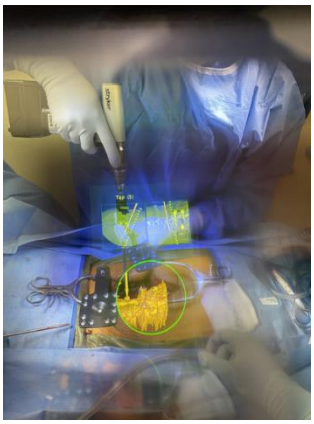

Figure 3: Augmented reality view of a surgery as seen through the xvision headset [39]

Augmedics xvision is a navigation system that feeds CT images of a patient through an augmented reality head-mounted display (HMD). The CT images are acquired through intraoperative CT scans and use a registration marker clamped onto the spinous process in order to match reflective markers to the CT images [40].

Philips ClarifEye

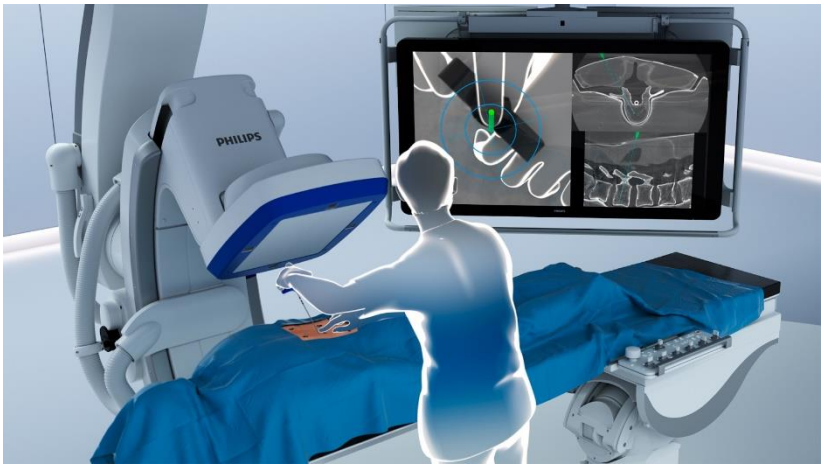

Figure 4: A model of the Philips ClarifEye in use [41]

Philips ClarifEye is a minimally invasive system that uses cone-beam CT (CBCT), which exposes patients to less radiation and obtains a 3D image of the patient. Unlike the Augmedics xvision, Philips ClarifEye uses 8-10 skin markers placed around the procedure point and only around 5 markers need to be seen to be accurately tracked. The markers are seen by four cameras that are integrated with the C-arm and a software generates a mesh pattern from them [42–46]. The 2D and 3D CT images along with the planned instrument trajectories are then displayed on external monitors.

SeaSpine 7D Surgical

Figure 5: The 7D Surgical system in use [47]

The SeaSpine 7D Surgical system uses optical topographic tracking to scan the patient and then uses machine learning to match the scan with preoperative scans of the patient. This system significantly reduces radiation exposure to the physicians and staff and uses a workflow called Flash Registration to quickly match the optical 3D surface image with the preoperative scans [48]. However, the optical topographic tracking requires that the bony anatomy like the spine be well exposed for the cameras [48,49]. To track the instruments, the system uses reflective markers which are then tracked with infrared cameras [48,50].

1.4 Physician Input

There are many different approaches to performing the epidural steroid injections and radiofrequency ablations and therefore each physician may have variations in their techniques and approach. To gain insight on different pain management therapies, four physicians (one from UCSD, two from UCI, and one from UCLA) were reached out to for their input. While their input provides invaluable perspective and insight, it should be noted that a sample size of four physicians is small. Also, since the physicians are from the University of California system, they have access to high quality equipment.

Two physicians expressed concern about radiation exposure while the two others did not. The two physicians who expressed concern work with fluoroscopy for many of their procedures whereas the two other physicians also perform other procedures. However, all four physicians mentioned the difficulty and long training periods that newer physicians need to go through to become ready to perform procedures on their own. Three of the physicians expressed interest in the potential of AR systems, especially for training newer physicians, but the fourth physician thought that augmented reality was more of a gimmick. Based on the physicians' responses, there is the potential for improvements to the way interventional pain management therapies and especially trainings are approached.

1.5 Need for Improvements to Pain Management Therapies

The technologies specified in section 1.3.2 are mainly used for invasive surgeries and complex procedures. However, their use would be excessive and expensive in interventional pain management therapies. The fluoroscopic C-arms used in pain management may range from

$25,000 to over $70,000 USD depending on their capabilities [51]. To give further perspective, the more advanced 7D Surgical system costs around $470,000 which is approximately a third of the cost for intraoperative CT-based navigation systems [50].

A limitation of fluoroscopy is that it is unable to get perfect axial views of the body [44,48]. Additionally, it is difficult to obtain clear images in the thoracic and thoracic-cervical spine due to the ribs and shoulders obscuring a clear view of the spine [48]. Another concern with fluoroscopy is that it exposes both the patient and physician to radiation. Besides the patient, the physicians and anyone inside the room wear lead aprons as a precaution, but it has been shown that standard lead aprons only block approximately one-third of scattered radiation [48,52]. If the physician performs these procedures frequently, then they will be exposed to a large amount of radiation over their work life. Other considerations for pain management therapies are to prioritize keeping the procedures as minimally invasive as possible and reducing the total procedure time.

In this thesis, an augmented reality navigation system utilizing preoperative magnetic resonance imaging (MRI) scans and non-invasive skin markers is proposed as a potential solution to address the current problems with interventional pain therapies. The preoperative MRI scan allows physicians to plan out the procedure in advance, get a clear model of the patient's anatomy with special attention to the nerves and blood vessels, and go straight into the procedure the day of the operation. The non-invasive skin markers are cheap to produce and enable accurate overlay of the 3D MRI model on top of the patient during the procedure. Lastly, augmented reality allows physicians to minimize attention shift and keep focused on the procedure at hand by having all the necessary information on and around the patient.

Chapter 2 Design

2.1 Augmented Reality Navigation System for Pain Management Therapies

As mentioned in Chapter 1, the augmented reality navigation system project is currently focused on pain management therapies. This narrows the scope of the project down to the epidural steroid injection and radiofrequency ablation procedures to help ensure that the project has a clear and well-defined outline that will produce quality results. To help visualize the overall project, Figure 6 depicts the roadmap of the entire project that is broken down into five main phases.

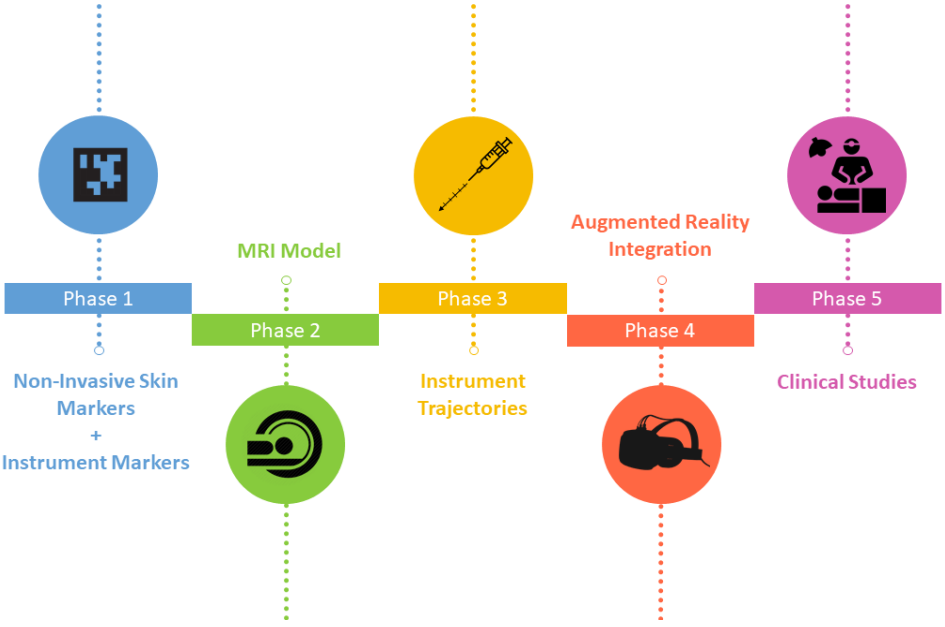

Figure 6: Roadmap of the Augmented Reality Navigation System Project

Phase 1: Non-Invasive Skin Markers and Instrument Markers

Phase 1 consists of non-invasive skin markers and instrument markers. The skin markers allow for the augmented reality model of the patient's anatomy to be accurately overlayed on top of the patient during the procedure. The instrument markers are used to confirm the needle tip locations within the patient's body.

Phase 2: MRI Model

Phase 2 consists of creating the 3D MRI model of the patient's anatomy for the pain management therapies. MRI was chosen over CT scans because it does not require the use of radiation and is also better at viewing soft tissues, specifically nerves and blood vessels [53–56].

Phase 3: Instrument Trajectories

With the MRI model, physicians will be able to see within the body. However, they still need to be able to see where their needles are located within the body. By developing instrument trajectories, physicians will be able to see recommended optimal needle trajectories and the actual needle locations within the patient.

Phase 4: Augmented Reality Integration

Phases 1-3 will be integrated into an augmented reality environment which will be seen via a headset with a heads-up display. The use of augmented reality will help prevent physician attention shift by having all the necessary information overlayed or near the procedure point.

Phase 5: Clinical Studies

If the augmented reality environment and headset are successfully merged with the markers, MRI model, and instrument trajectories, then comprehensive testing can begin with surgical dummies, continue with cadavers, and then finally proceed to clinical trials.

The above description was a brief overview of the entire project. There are overlaps between the phases, and each phase also includes many different subprojects that have not been listed. The phases and subprojects may also change in the future according to further research and new findings.

2.2 Thesis Overview: Non-Invasive Skin Markers

2.2.1 Marker Tracking

Many different registration methods can be used in localization and tracking. Such methods include electromagnets, reflective markers, and skin markers and each method has its own advantages and disadvantages. Electromagnetic (EM) systems utilize electromagnetic sensors and do not require a line-of-sight to the sensors. However, those sensors are susceptible to noise from nearby metals causing them to have less accuracy compared to optical systems [48]. Reflective systems utilize near infrared (NIR) reflective spherical markers; these markers are very accurate but require the use of near infrared lights and filters [57]. They also usually use a reference frame that is attached to the spinous process and if that frame is accidentally moved from its original position, it would require a long time to recalibrate the system [44,48]. Skin markers are placed around the procedure point and therefore allow for more consistent tracking at multiple levels of the body compared to fixed reference frames [58]. They can come as circles or squares but since circles usually only give one correspondence point whereas square markers give four, square markers are more preferred in tracking [59]. Square markers are used in many applications such as human-computer interaction, AR/VR, robotics, and tracking surgical instruments [60].

2.2.2 Non-Invasive Skin Markers

Non-invasive skin markers are placed on the patient before the preoperative MRI scan and show up on the MRI images. After the scan, the patient goes home for up to two weeks with the markers still attached. During this time, a 3D model of the patient's anatomy will be constructed and analyzed to help the physician determine the best approach for the procedure. When the patient comes in for the procedure and lays down on the operating table, cameras will locate the markers

and align them with the markers found on the MRI model to create the augmented reality MRI overlay.

There are many different factors that need to be considered for the markers used in this research project. For example, bigger markers would be easier to track, and any potential warping would be relatively smaller compared to the same warping with smaller markers. However, bigger markers are a bigger target on the patient's back and therefore the larger size may make it easier for patients to accidentally hit or peel the markers.

Skin markers were selected because they need to remain on the patient for up to two weeks without shifting and need to allow accurate tracking during the time of operation. The skin markers are generally thinner and less obtrusive than the other markers, thus making them more convenient to wear. An added benefit is that skin markers are a non-invasive method of tracking which helps keep the interventional pain therapy procedures as minimally invasive as possible. A depiction of the non-invasive skin markers in the operating room is shown in Figure 7.

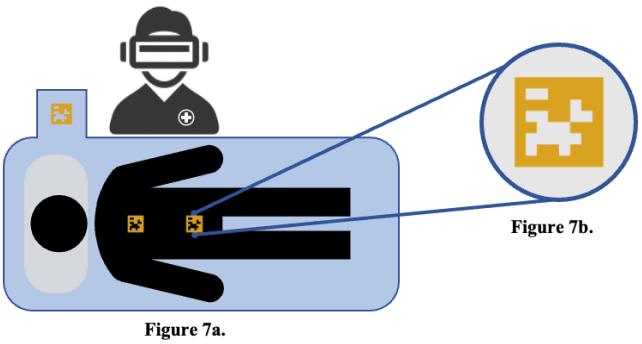

Figure 7: (a) Depiction of the skin markers on the patient and operating table and (b) a close up view of one of the skin markers

The main consideration for using skin markers is whether they can keep the same tracking accuracy from before the patient undergoes the MRI scan to during the procedure itself. But in order to more accurately test the performance of the non-invasive skin markers in the operating room, there is a need to simulate potential body motions of the patient on the operating table.

Chapter 3: XYZ Marker Platform

As mentioned in Chapter 2, there is a need to have a good simulation of the patient and their potential body motions on the operating table. The patient may be asked by the physician to shift along the operating table or they may flinch in response to the needle insertions. Also, the patient will naturally have their chest expand and compress during respiration. An XYZ platform was chosen to simulate those body movements in the skin marker tracking experiments. Pictures of the computer-aided design and constructed XYZ platform can be seen in Figures 8 and 9.

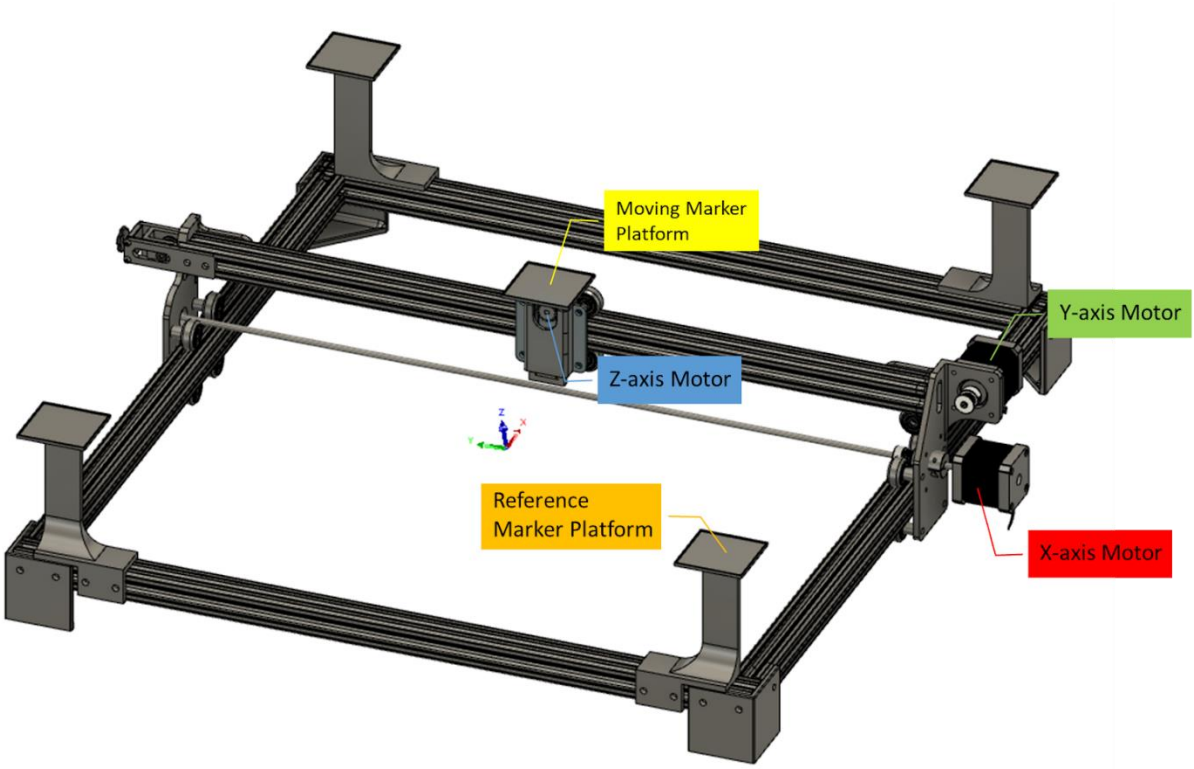

Figure 8: CAD Model of the XYZ Platform

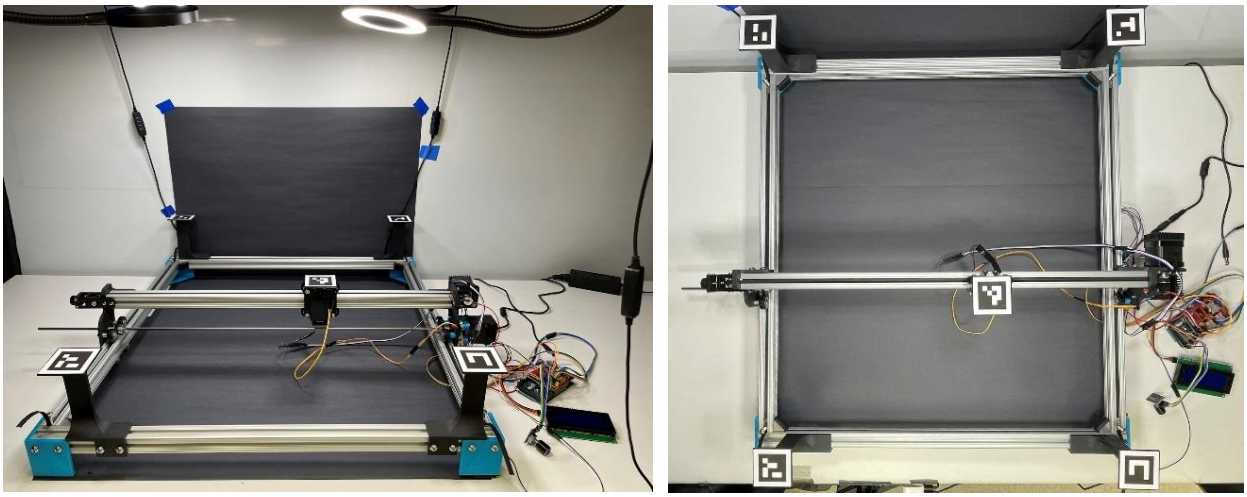

Figure 9: XYZ Platform with (a) top-front view and (b) top view

The size of the XYZ platform is approximately 50x50 cm, which is large enough to study most people since the biacromial width is approximately 41.1 cm for males and 36.7 cm for females [61].

The perimeter of the XYZ platform represents the operating table on which reference markers would be placed as fixed points in space while the moving marker platform in the middle represents the moving non-invasive skin markers on the patient. For simplicity during the experiments, there is only one moving marker.

The XYZ platform uses three stepper motors to move each respective axis. Stepper motors were chosen because they have good low speed torques, strong holding torque, and have non-cumulative error. Microstepping was added to the stepper motors in order to make the motors run more smoothly, to ensure that the marker would also have smooth movements.

Foam pads were added underneath the platform to dampen any potential vibrations that could affect the markers. Black drapes were also added around the whole experiment table to help isolate the whole setup from external variations. Lastly, six different lamps were positioned around the XYZ platform in order to provide even lighting. The pads, drapes, and lights were all included in the setup so that only the desired variable would be noticeably changed during the experiments.

3.1 Platform Functions

The XYZ platform contains many different functions with which it serves to mimic patient movements, create controlled patterns for testing, and to increase the convenience of the user. The functions are programmed and selected using an Arduino and a corresponding menu.

Figure 10: This is the main menu used to control the Arduino and XYZ Platform.

Homing

A characteristic of stepper motors is that they do not retain their position when they are powered down. Instead, they set their current position to zero whenever they are powered on. To address this, it was necessary to have a homing function so that the marker platform can know its actual position in the XYZ platform. The homing function was integrated within all other functions besides manual movement.

Distance and Speed

There are many reasons why a patient may move during the procedure. The physician may ask the patient to shift along the table to a more optimal position or the patient may react in pain to the needle insertion. But since the physician waits for the patient's body movements to stabilize before starting or resuming the procedure, the distance and speed of movements do not have a large impact. However, these functions were still included to help characterize the marker tracking.

Breathing

During the procedure, the physician tries to keep the patient as still as possible. However, the patient's chest expands and compresses during respiration. Therefore, the Z axis on the XYZ platform was used to mimic chest expansion and compression. There are options to change both the breathing rate and the amount of chest expansion and compression. During this pattern, the marker platform moves to the middle of the XYZ platform and then cycles through the inputted breathing rate at the specified chest distance for one full minute.

Tuning

In the case that the timing belts loosened over time or the platform is reassembled, a function was included to recalibrate the stepper motors. Currently, the X and Y stepper motors are set to 40 mm per revolution and the Z stepper motor is set to 47.5 mm per revolution.

Manual

For quality control and testing purposes, a manual setting was included so that each of the axes could be individually adjusted. For additional convenience, an option was also included to individually home each axis.

3.2 XYZ Platform Quality Control Methods

Before the XYZ platform can be used as the ground truth in the marker tracking experiments, it must first undergo quality control to verify the platform, ensuring that it moves the same distances and speeds as intended.

3.2.1 Distance Analysis Method

To analyze the distances, the XYZ platform was moved in each of the X, Y, and Z axes and measured with a caliper. Two types of tests were conducted to analyze the distance: Rest Test

and Increment Test. Both tests were conducted to view the marker platform from different perspectives.

Reset Test

This test is called the reset test because after each movement, the marker platform is "homed back" to its original position and then set to move a slightly larger distance afterwards. For example, the marker platform is set to move 10 mm in the X direction. After it moves 10 mm, the marker platform is homed and then set to move 20 mm. For the X and Y directions, the distances are set from 10 mm to 300 mm with 10 mm spacings. In the Z direction, the distances are set from 3 mm to 45 mm with 3 mm spacings. Each test was repeated three times in the X and Y directions and six times in the Z direction to get 90 sample points each.

Increment Test

This test is called the increment test because the marker platform does not continuously move the full distance nor does it home after each movement. In the X and Y directions, the marker platform moves in 10 mm increments until it reaches 300 mm. In the Z direction, the marker platform moves in 3 mm increments until it reaches 45 mm. Like in the reset test, the X and Y direction tests were repeated three times and the Z direction test was repeated six times.

3.2.2 Speed Analysis Method

Videos were taken with a top view for the X and Y directions and a front view for the Z direction in the speed tests. For the X and Y directions, the marker platform was moved at 10, 15, and 20 mm per second and different distances of 120, 240, and 480 mm. For the Z direction, the marker platform was moved at 10, 15, and 20 cycles per minute for one or three centimeters. This is to simulate different breathing rates and chest expansion/compressions. After the videos were taken, they were analyzed frame by frame to determine the start and stop times of each experiment.

3.3 XYZ Platform Errors

3.3.1 Distance Errors

Reset Test

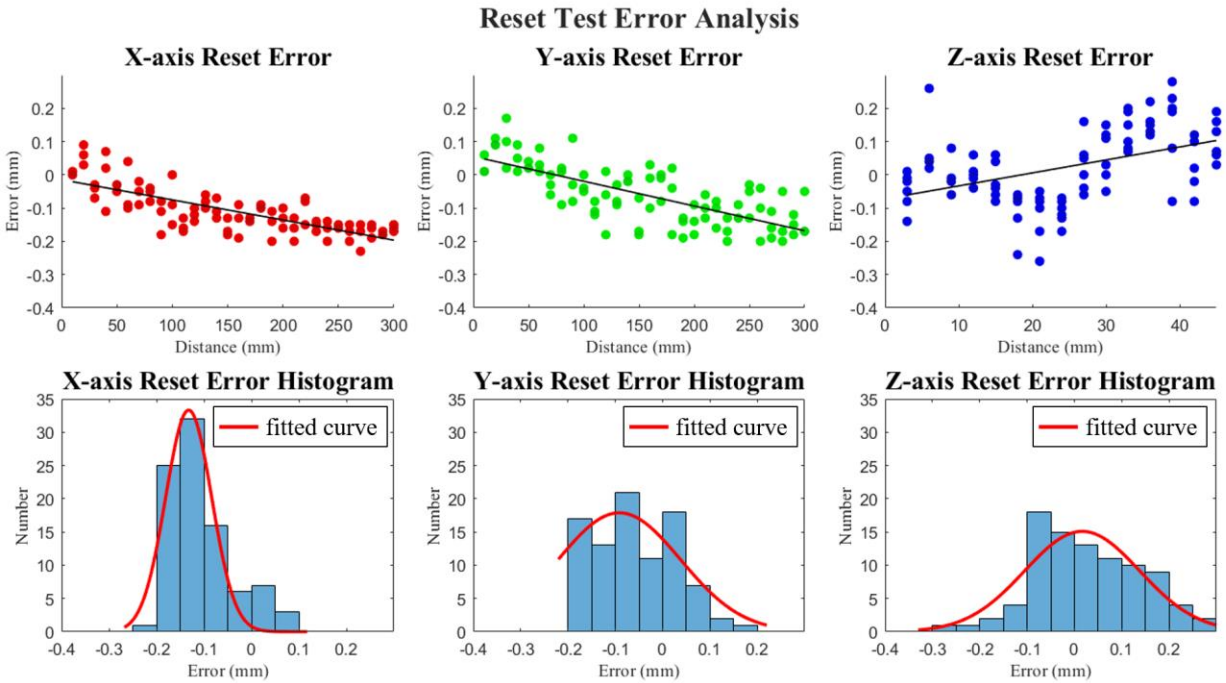

Figure 11: Scatter plots and histograms of the Reset Tests for each of the X, Y, and Z axis.

Table 2: Error Table of the X, Y, and Z Directions in the Reset Test

	X	Y	Z
Mean error	-0.11 ± 0.07 mm	-0.06 ± 0.09 mm	0.02 ± 0.11 mm
Line of Best Fit	-0.0006x – 0.0146	-0.0007x + 0.0552	0.0037x – 0.0723
R^2	0.5926	0.54614	0.2079

Increment Test

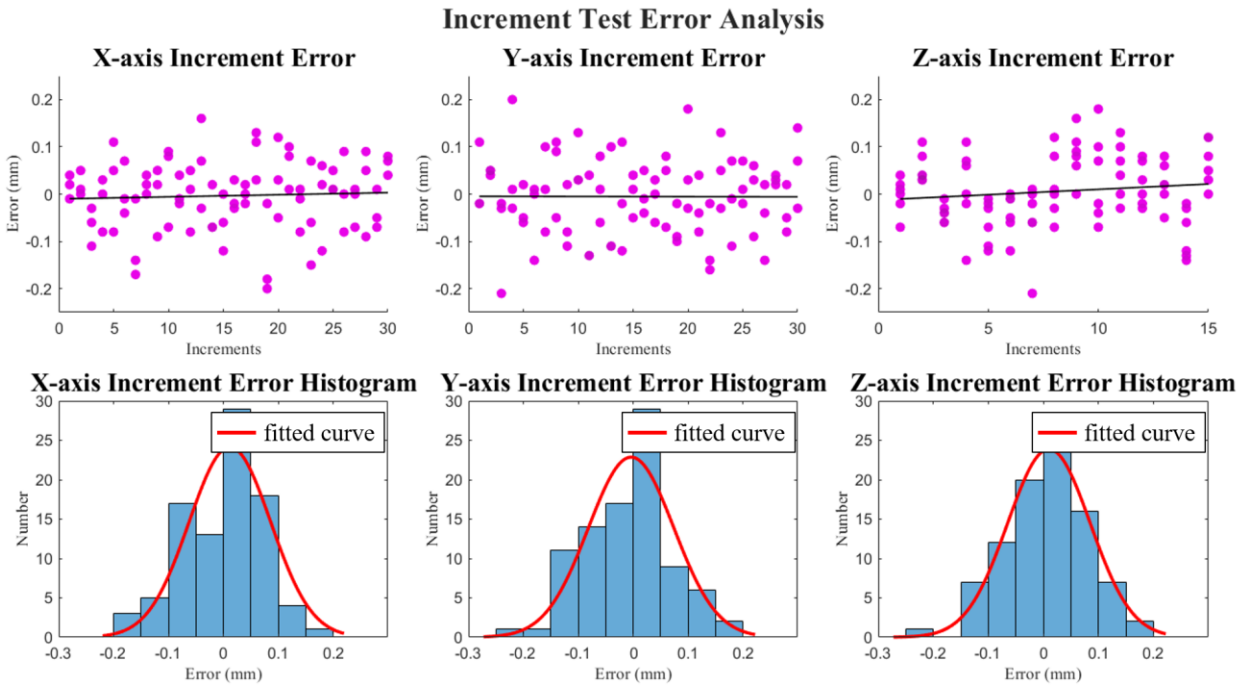

Figure 12: Scatter plots and histograms of the Increment Tests for each of the X, Y, and Z axis.

Table 3: Error Table of the X, Y, and Z Directions in the Increment Test

	X	Y	Z
Mean error	-0.01 ± 0.07 mm	-0.01 ± 0.08 mm	0.01 ± 0.07 mm
Line of best fit	0.000044x – 0.0102	-0.0000044x – 0.0045	0.00052x – 0.0077
R^2	0.0028	0.000023	0.0108

3.3.2 Speed Errors

Table 4: Marker Platform Speeds in the X and Y Directions in Millimeters per Second

	120 mm at 10 mm/s	120 mm at 15 mm/s	120 mm at 20 mm/s
X-direction	9.89 ± 0.02	14.88 ± 0.03	19.73 ± 0.04
Y-direction	9.88 ± 0.02	14.92 ± 0.03	19.77 ± 0.04
	240 mm at 10 mm/s	240 mm at 15mm/s	240 mm at 20 mm/s
X-direction	9.88 ± 0.01	14.88 ± 0.01	19.73 ± 0.02
Y-direction	9.87 ± 0.01	14.9 ± 0.02	19.74 ± 0.02
	480 mm at 10 mm/s	480 mm at 15mm/s	480 mm at 20 mm/s
X-direction	9.88 ± 0.01	14.87 ± 0.01	19.73 ± 0.01
Y-direction	9.87 ± 0.01	14.89 ± 0.01	19.72 ± 0.01

Table 5: Marker Platform Speeds in the Z Direction in Cycles per Minute

	1 cm – 10 cycles/min	1 cm – 15 cycles/min	1 cm – 20 cycles/min
Z-direction	9.98 ± 0.02	14.94 ± 0.02	19.97 ± 0.02
	3 cm – 10 cycles/min	3 cm – 15 cycles/min	3 cm – 20 cycles/min
Z-direction	9.95 ± 0.02	14.92 ± 0.02	19.87 ± 0.02

3.4 Discussion

3.4.1 Distance Errors Discussion

In the Reset Test, as seen in Figure 11, both X and Y directions seem to have an undershoot since the lines of best fit show a moderate negative correlation between distance and error and the histograms show a right skew. The right skew shows that most of the errors are negative and therefore the X and Y directions may be moving slightly less than intended. An undershoot of 0.0006 or 0.0007 mm would mean that one revolution of the X or Y stepper motors would undershoot approximately 0.024 mm, or 3.84 steps out of 6400. There may be a plateau in the

errors as distance increases but that cannot be determined until a larger caliper or a new method of analyzing the XYZ platform is obtained.

In the Increment Test, as seen in Figure 12, there does not appear to be an undershoot in the X or Y directions and there appears to be a Gaussian distribution of errors. This suggests that the marker platform performs randomly no matter its location on the X or Y axes and that there is no noticeable flaw or bias in the XYZ platform construction for the X and Y directions. Therefore, both the Reset and Increment Tests together suggest that the marker platform slightly undershoots in the X and Y directions.

Both the Reset and Increment Tests show a wave pattern as the marker platform moves along the Z axis. This suggests a flaw in the rack and pinion mechanism used for moving the marker platform vertically. This can be explained by the tolerance between the rack and the casing of the mechanism. As the gear rotates, the rack slightly moves sideways and causes an oscillation pattern. This was confirmed later by analysis of the front view videos frame by frame. However, despite the oscillations, the marker platform still only had errors of 0.02 ± 0.11 mm in the Reset Test and 0.01 ± 0.07 mm in the Increment Test. Besides the wave pattern, the Rest Test suggests that the Z direction is overshooting due to the left skew and positive line of best fit. But in order to accurately determine if the Z direction is actually overshooting and to what degree, the tolerance of the rack and gear mechanism should be tightened.

3.4.2 Speed Errors Discussion

To determine the errors, the estimated distance errors needed to be used in the error propagation. The time error was assumed to be one frame, or $1/60^{th}$ of a second.

As seen in Table 4, the marker platform slightly underperformed the intended speeds in the X and Y directions. The ratio of actual to expected speed was 0.985 or greater for every iteration.

The difference in the actual speeds from the intended speeds could be due to a little bit of slack in the timing belt. The XYZ platform was assembled to have slack in the timing belts to prevent over-tightening. Over-tightening of the belts would have caused the belts to creep over time and loosen in the future. This would introduce false expectations of the XYZ platform performance until the platform was reanalyzed.

As seen in Table 5, the X, Y, and Z directions all had slightly lower than expected speeds. However, compared to the X and Y directions, the Z direction speed had a higher ratio of actual to expected speed of 0.99 or more for all iterations. The underperformance from the expected speed in the Z direction could have been due to the tolerance between the rack and pinion, where some of the intended vertical motion was converted to horizontal motion.

3.5 XYZ Platform Conclusion

Since both the distance and speed of the XYZ platform were largely characterized, it was determined that the XYZ platform would serve its purpose in the marker tracking experiments. The focus of the non-invasive skin markers project is the marker tracking experiments, not the XYZ platform itself. Therefore, the XYZ platform errors can be accounted for when conducting the marker tracking experiments.

Chapter 4 Marker Tracking Experiment Setup

4.1 QR Codes and ArUco Codes

Square skin markers are preferred over circular markers due to their ability to give multiple points of correspondence. The most widely used and recognized square marker is the Quick Response Code or QR code and its variants.

QR Codes

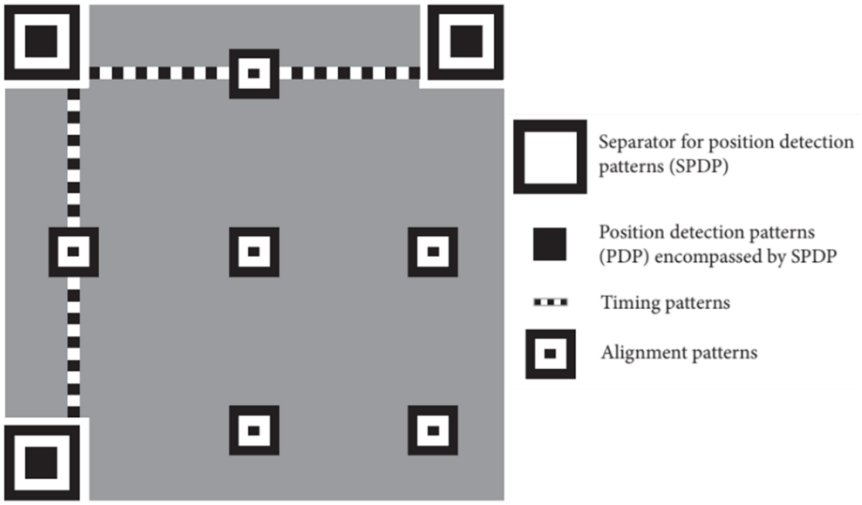

Figure 13: Structure of a basic QR code [62]

The QR code is a 2D matrix barcode made up of function graphics and an encoding region. The function graphics, as seen in Figure 7, include finder patterns to recognize and see the orientation of the QR code, timing patterns to determine the width of the code, and alignment patterns to correct for distortion of the QR code. The encoding region includes the version information, error correction code, and data of up to 7,089 numeric characters (*i.e.,* 3Kb of data) [63,64]. QR codes are convenient to use for tracking purposes because they are inexpensive, have high storage capacity, and can still be tracked up to 30% damage [62,64–68]. They also

require low computational power and the finder patterns allow for camera pose estimation [59,60,62]. However, image blur and deformations, and changes in the environment can reduce the accuracy of tracking or cause the QR code to become unrecognizable and untrackable [62,65].

ArUco Codes

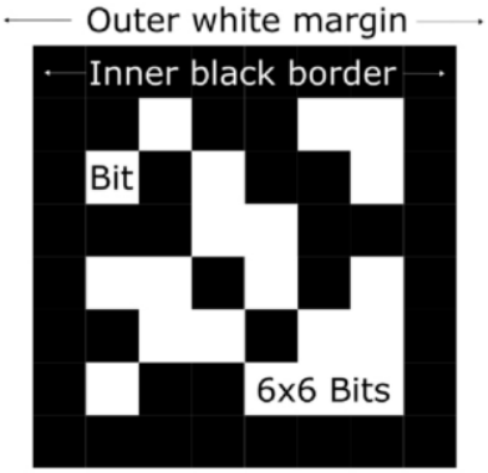

Figure 14: Example of an ArUco code [69]

ArUco codes are similar to QR codes but, as seen in Figure 8, contain far fewer bits than QR codes and therefore encode less information. Unlike QR codes, the bit grid of the ArUco code is used for identification and does not hold any extra information [69]. However, the ArUco codes are used purely for tracking purposes and therefore hold higher accuracy than QR codes while still being low-cost to produce [69]. The use of ArUco codes is not as widespread compared to QR codes and therefore needs more specialized systems that can recognize them. However, the ArUco codes are open sourced and well-documented, which makes them more convenient to use compared to other square markers [69].

4.2 Experimental Setup

From lighting, to camera distance, to line-of-sight obstructions, there are many potential factors that may affect the accuracy of ArUco code tracking [60,69]. It is imperative to determine the most salient factors so that they can be addressed and minimized in the operating room. The experiments are conducted within the "closed system" (specified in Chapter 3) in order to reduce the chance of any outside interference and each experiment tests one different variable at a time.

The experimental equipment is divided into three categories: ArUco code, camera, and operating room. By closely observing how each variable can affect marker tracking, it will be easier to make a more informed decision when creating a marker for a certain patient given certain housing and operating room conditions.

4.2.1 ArUco Code Experiments

It is important to characterize the properties of the ArUco code and how each property may influence the overall tracking of the marker. Having a good understanding of the ArUco code properties would allow physicians to choose the best marker for a patient.

Marker movement speed

During a procedure, the patient will be continually moving their chest up and down during respiration. Also, they may flinch in response to the needle insertion or be asked by the physician to shift on the operating table. It is important that the skin markers can still be accurately tracked despite those movements and speeds. The markers were tested at velocities of 10, 15, and 20 mm/s. Higher speeds could not be reliably tested due to the limits of the stepper motors and the Arduino library used to control those motors.

Marker pixel density

The ArUco code library includes 4x4, 5x5, 6x6, and 7x7 bit codes. The increased pixel density helps increase the resolution of the codes but the resulting smaller pixels may be harder to spot by the camera. Figure 15 shows examples of 4x4, 5x5, 6x6, and 7x7 ArUco codes, each of the identity (ID) 0.

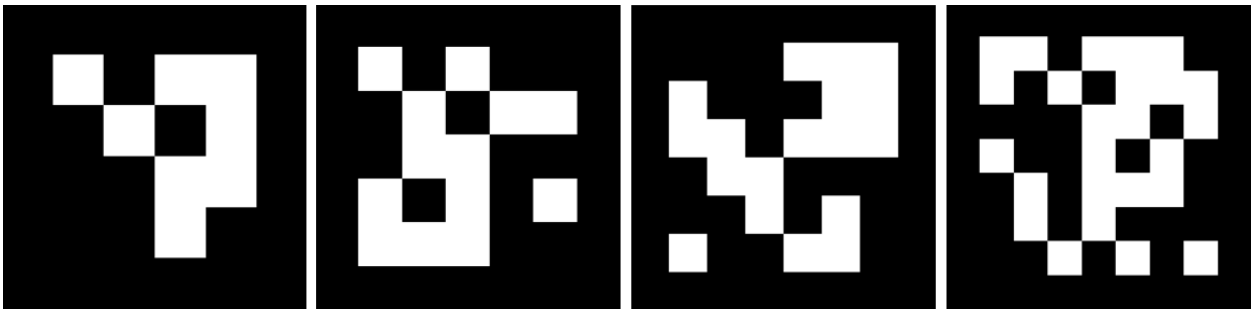

Figure 15: Example of different marker pixel densities each with ID 0.

Marker size

The markers were tested at 2, 3, 4, and 5 cm square sizes. These sizes do not include the white contrast borders. Increased marker sizes can help the markers be more easily recognized and tracked but may also be more inconvenient to the patient.

Marker border thickness

The AruCo codes usually have a white border around them. The border does not serve as part of the identification of the code but helps provide a high contrast border. Tests were conducted with borders of 0, 0.5, 1, 1.5, and 2 white pixels.

Reference markers

Reference markers were placed on the operating table to serve as fixed points in real space with which the non-invasive skin markers and subsequent AR model will be referenced to. Tests were conducted with 1 through 4 reference markers.

Marker contrast

The best contrast for a marker is white against black. However, in real life applications, there may be situations where the marker has less contrast, perhaps due to a patient wanting different color combinations or the marker getting dirty or wearing off over time. The ArUco codes were tested at Grayscales 0%, 25%, 50%, and 75%.

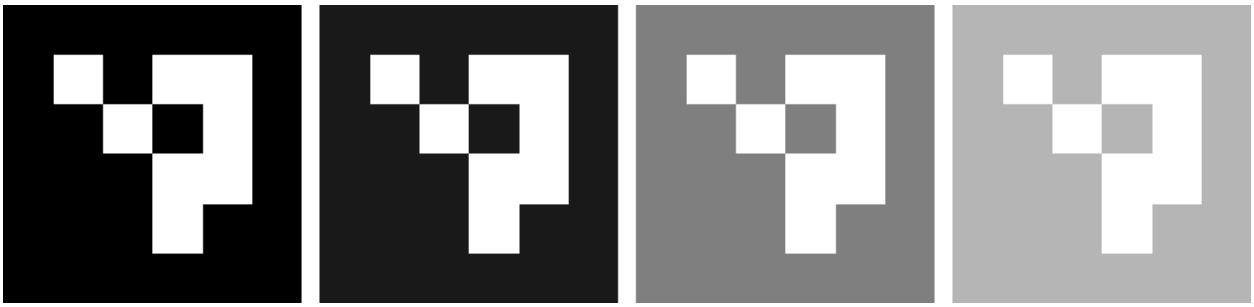

Figure 16: ArUco codes at Grayscale 0%, 25%, 50%, and 75% respectively.

Marker angle and marker warping

On the operating table, the patient may be oriented in various ways depending on the physician. This will affect how the non-invasive skin markers will be oriented with respect to the reference markers. Also, the skin markers may be placed on parts of the body with a natural curve, such as directly over the spine. The marker was tested at 0°, 15°, 45°, and 60° in the angle test and at 1 cm concave, 1 cm convex, 25% stretch, or 25% compression in the warp tests.

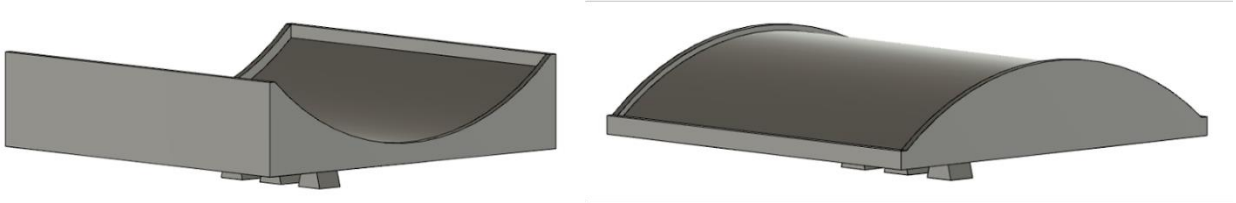

Figure 17: Concave and Convex Marker Platforms

4.2.2 Camera Experiments

The proposed augmented reality navigation system utilizes optical tracking of the skin markers in order to map the 3D MRI model on top of the patient. As such, it is important to understand the types of cameras that can be used within the procedure and how they should be placed relative to the patient and markers. For simplicity, only one camera was used but a multi-camera setup will be used as the project progresses and improves.

Camera resolution and frames per second (fps)

The camera was tested at 1080p and 4K resolutions at 30 and 60 fps. Increased resolution and frame rate may make it easier to accurately process the videos but will also lead to increased memory and therefore processing time. There needs to be a balance between both accuracy and processing time if this system is to be used during an actual and live procedure.

Camera distance

If external cameras are used, then the camera distance to the procedure may vary according to how they are set up. If the cameras are integrated into a headset, then the distance to the procedure point may change throughout the procedure if the physician wants to get a different view of the patient. The camera was placed at 50, 60, and 70 cm during the tests.

Camera angle

This is similar to the marker angles but camera angle changes cause both the skin and reference markers to be angled in the camera's perspective, not just the skin markers. However, since the use of one camera has ambiguities and singularities in 3D tracking [70], it was decided to not conduct the camera angle experiments. This variable will be tested in a future study using a multiple camera setup.

4.2.3 Operating Room Experiments

The operating room can contain many different instruments, equipment, and staff that could all potentially influence the marker tracking. Two different operating rooms can be seen in Figure 18. The first room, Figure 18(a), has a lot of equipment and screens near the table and has warmer lighting while the second room, Figure 18(b), is more simplistic and has whiter lighting. It should also be noted that these two operating rooms are from a first-world country and therefore would vastly differ from those in less wealthy countries.

Figure 18: Two different operating rooms, (a) from St. Luke's University Hospital and (b) from Saint Louis University Hospital [71,72].

Lighting

Hospitals and operating rooms may vary greatly depending on their available budget. As seen in Figure 18, this can result in different lighting, from light temperature to light intensity. Therefore, it is important to test how these different lighting conditions may affect the marker tracking. First, light was tested at white, warm-white, and warm colors (or 6000, 4500, and 3000K respectively). Then the light intensity was measured at 1000, 700, 500, and 200 lux.

Uneven Lighting

This is similar to the lighting experiment, but the markers will be unevenly illuminated. This experiment simulates situations where a physician may move around and block a light source or operating rooms where light sources are unevenly distributed. To control this, the two side lights

were turned off. Then each subsequent test would turn off one corner light at a time until one light remained.

Line of sight obstruction

One of the biggest challenges of optical tracking systems is if the line-of-sight from the cameras to the markers is obstructed [50,68,73]. Obstruction could be a partial or complete covering of the marker from the cameras' perspective. In an operating room, such as in Figure 19, there are many factors that could obscure vision of the markers, especially if there are multiple people around the patient.

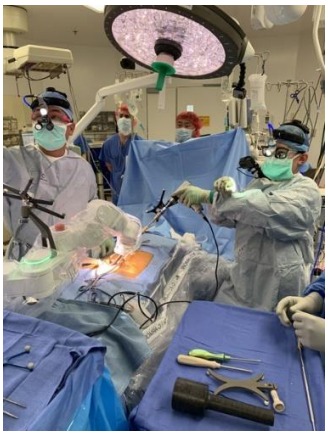

Figure 19: An operating room at UC San Diego Health [74].

The markers were covered with a 0, 0.5, 1, or 1.5 bit thick strip that was moved across the marker top-to-bottom, left-to-right, and diagonally.

Glare

Depending on the skin marker's material, there may be glare from light sources around the operating room especially if the marker is glossy. This is an important variable to consider but will not be tested until a future study due to the dependence on the marker material.

4.2.4 Experiment Default Parameters

In order to determine the effects of each variable on marker tracking, there needs to be a set of default parameters used throughout the experiments for consistency for better comparisons. The default parameters are shown in Table 6 and each experiment will be repeated three trials each. The XYZ platform movement pattern is a square and diagonals as shown in Figure 20. In Chapter 5, the parameters with bolded font represent the experiments with default parameters.

Table 6: Experiment Default Parameters

Marker Platform Speed	10 mm/s
Reference Marker	1 marker
Pixel Density	4x4 pixels
Pixel Size	4 cm
White Border	1 bit
Marker Contrast	Grayscale 0%
Angle	0°
Warping	No Warp
Camera Distance	60 cm
Camera Resolution, Fps	1080p, 60 fps
Camera Angle	90°
Lamps	All on at 1000 Lux
Line-of-Sight Obstruction	No Line-of-Sight Obstruction
Shadows	No Shadows
XYZ Platform Movement Pattern	Square with Diagonals

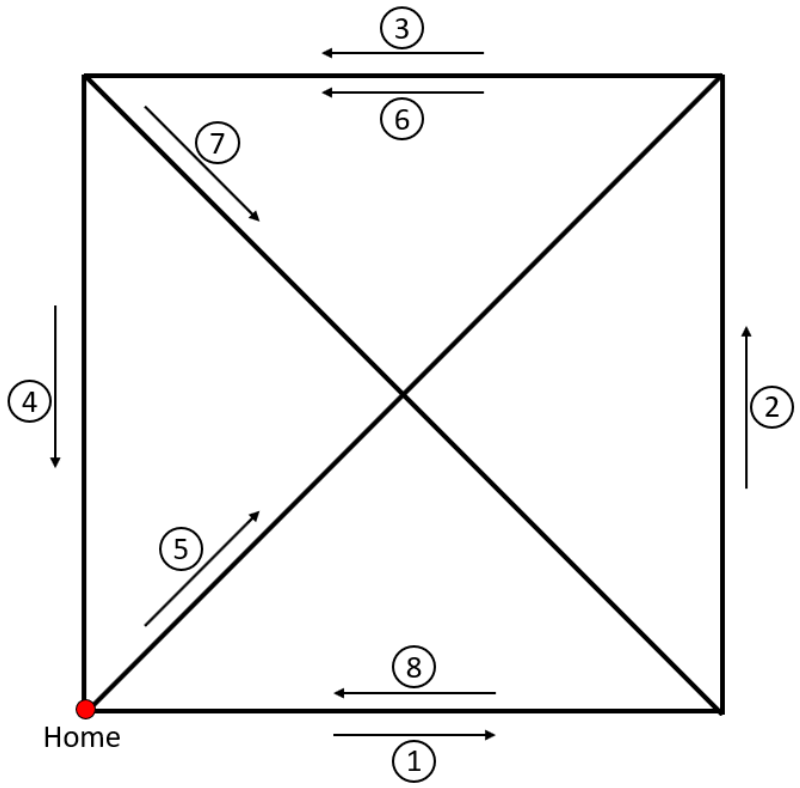

Figure 20: XYZ platform movement pattern. 1-8 corresponds to the order of travel.

Chapter 5 Experimental Results and Discussion

5.1 Data Analysis

Coordinate data was pulled from video recordings that served as input to a Python and openCV tracking algorithm and was then exported to MATLAB for analysis. One of the benefits of using ArUco codes is their open source and well documented dictionary. The GitHub repository from GSNCodes for Python and openCV was used as the skeleton of the program to detect the ArUco codes [75]. The coordinate data was exported to MATLAB for post-processing to detect and filter outliers and false positives. After filtering, the coordinates were matched with those of the coded default XYZ platform pattern to find the tracking errors.

An example of the marker as it moves with the XYZ platform is shown in Figure 21(a); each color corresponds to a direction movement of the XYZ platform. The corresponding heatmap of position errors along the marker path in Figure 21(a) is shown in Figure 21(b). As there are many graphs per variable tested, the error heatmaps will be consolidated to tables. The corresponding Figures are found in the Appendix (Figures A1-26).

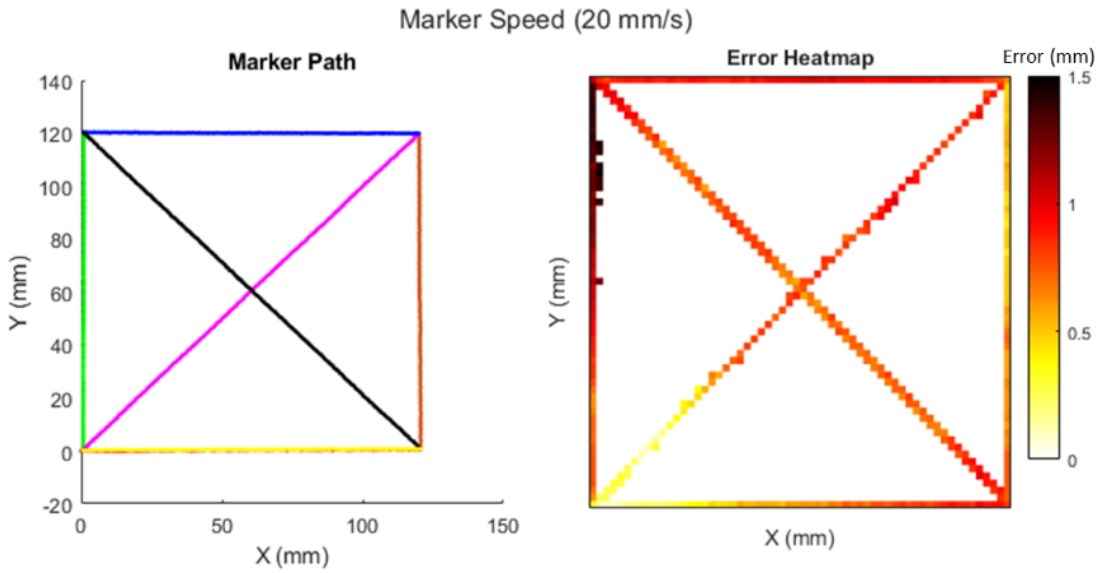

Figure 21: (a) The Plotted Coordinates of the Marker Moving at 10 mm/s. (b) The Error Heatmap Along the XYZ Platform Movement Pattern.

5.2 Results

5.2.1 ArUco Code Results

Marker Movement Speed

Table 7: Error Results (in mm) for XYZ Platform Speeds

	Trial 1	Trial 2	Trial 3
10 mm/s	1.04 ± 0.68	0.79 ± 0.45	0.65 ± 0.40
15 mm/s	0.95 ± 0.34	1.05 ± 0.47	0.90 ± 0.46
20 mm/s	0.74 ± 0.31	0.75 ± 0.27	0.72 ± 0.23

Number of Reference Markers

Table 8: Error Results (in mm) for Numbers of Reference Markers

	Trial 1	Trial 2	Trial 3
1 Reference Marker	0.95 ± 0.35	1.00 ± 0.38	0.83 ± 0.33
2 Reference Markers	0.83 ± 0.34	0.83 ± 0.34	0.86 ± 0.32
3 Reference Markers	1.03 ± 0.42	0.77 ± 0.34	0.77 ± 0.30
4 Reference Markers	0.82 ± 0.33	0.82 ± 0.31	0.96 ± 0.34

Pixel Density

Table 9: Error Results (in mm) for Pixel Densities

	Trial 1	Trial 2	Trial 3
4x4 Pixels	0.86 ± 0.35	0.95 ± 0.36	0.79 ± 0.30
5x5 Pixels	0.84 ± 0.31	1.04 ± 0.45	0.96 ± 0.35
6x6 Pixels	0.18% Detected	0.65% Detected	0.96% Detected
7x7 Pixels	0% Detected	0% Detected	0% Detected

The red highlighted text emphasizes the parameters that could not be tracked throughout the experiments. A percent detection rate replaced the mean error and standard deviation to provide an alternative metric of evaluation.

Marker Size

Table 10: Error Results (in mm) for Marker Sizes

	Trial 1	Trial 2	Trial 3
2 cm	0.46 ± 0.22	0.60 ± 0.29	0.55 ± 0.29
3 cm	0.70 ± 0.34	0.99 ± 0.56	0.80 ± 0.35
4 cm	0.98 ± 0.51	1.12 ± 0.45	0.91 ± 0.27
5 cm	0.91 ± 0.42	0.74 ± 0.27	0.79 ± 0.31

Marker Borders

Table 11: Error Results (in mm) for Border Thicknesses

	Trial 1	Trial 2	Trial 3
0 bits	0% Detected	0% Detected	0% Detected
0.5 bits	3.14% Detected	3.63% Detected	3.56% Detected
1 bit	1.22 ± 0.64	1.02 ± 0.41	0.90 ± 0.41
1.5 bits	1.03 ± 0.42	0.95 ± 0.38	0.89 ± 0.37
2 bits	0.98 ± 0.39	0.99 ± 0.38	0.88 ± 0.36

Marker Contrast

Table 12: Error Results (in mm) for Contrasts by Grayscale

	Trial 1	Trial 2	Trial 3
Grayscale 0%	0.60 ± 0.31	0.83 ± 0.48	0.67 ± 0.37
Grayscale 25%	0.80 ± 0.36	0.77 ± 0.33	0.75 ± 0.33
Grayscale 50%	0.70 ± 0.32	0.81 ± 0.39	0.85 ± 0.39
Grayscale 75%	0.80 ± 0.39	0.92 ± 0.49	0.75 ± 0.30

Marker Angle

Table 13: Error Results (in mm) for Marker Angles

	Trial 1	Trial 2	Trial 3
0° Slant	0.84 ± 0.41	0.75 ± 0.37	0.88 ± 0.38
15° Slant	1.53 ± 0.58	1.45 ± 0.53	1.41 ± 0.56
45° Slant	2.96 ± 1.20	3.21 ± 1.38	3.16 ± 1.27
60° Slant	4.93 ± 2.06	4.23 ± 2.09	4.85 ± 2.07

Marker Warping

Table 14: Error Results (in mm) for Warping

	Trial 1	Trial 2	Trial 3
No Warp	0.97 ± 0.41	0.98 ± 0.41	0.95 ± 0.35
1 cm Concave	1.73 ± 0.66	1.71 ± 0.63	1.61 ± 0.61
1 cm Convex	1.45 ± 0.57	1.70 ± 0.65	1.62 ± 0.66
25% Stretch	0.98 ± 0.41	0.94 ± 0.35	0.82 ± 0.34
25% Compress	1.03 ± 0.42	0.94 ± 0.35	0.81 ± 0.32

5.2.2 Camera Setup Results

Camera Distance

Table 15: Error Results (in mm) for Camera Distances

	Trial 1	Trial 2	Trial 3
50 cm	0.80 ± 0.49	0.66 ± 0.35	0.65 ± 0.34
60 cm	0.95 ± 0.35	1.00 ± 0.38	0.83 ± 0.33
70 cm	1.24 ± 0.49	1.43 ± 0.57	1.33 ± 0.52

Camera Resolution and Frames per Second (fps)

Table 16: Error Results (in mm) for Camera Resolutions and Fps

	Trial 1	Trial 2	Trial 3
1080p, 30 fps	1.26 ± 0.69	1.12 ± 0.59	1.15 ± 0.59
1080p, 60 fps	0.75 ± 0.35	0.95 ± 0.42	0.80 ± 0.29
4K, 30 fps	1.47 ± 0.74	1.48 ± 0.71	1.71 ± 0.83
4K, 60 fps	0.72 ± 0.34	0.85 ± 0.43	0.80 ± 0.39

5.2.3 Operating Room Results

Light Temperature

Table 17: Error Results (in mm) for Light Temperature

	Trial 1	Trial 2	Trial 3
6000 K	0.76 ± 0.34	0.97 ± 0.43	0.78 ± 0.30
4500 K	0.98 ± 0.40	0.79 ± 0.31	0.88 ± 0.42
3000 K	0.93 ± 0.48	0.85 ± 0.40	0.93 ± 0.35

Lighting Intensity

Table 18: Error Results (in mm) for Light Intensity

	Trial 1	Trial 2	Trial 3
1000 lux	0.75 ± 0.31	0.96 ± 0.43	0.78 ± 0.43
700 lux	0.88 ± 0.37	1.05 ± 0.46	1.07 ± 0.36
500 lux	0.97 ± 0.38	0.86 ± 0.30	0.92 ± 0.38
200 lux	1.13 ± 0.47	1.07 ± 0.38	0.82 ± 0.31

Uneven Lighting

Table 19: Error Results (in mm) for Uneven Lighting

	Trial 1	Trial 2	Trial 3
0 lights off	0.71 ± 0.29	0.83 ± 0.39	1.10 ± 0.56
2 side lights off	0.63 ± 0.25	0.93 ± 0.38	0.78 ± 0.31
1 corner light off	1.11 ± 0.44	0.82 ± 0.29	0.93 ± 0.31
2 corner lights off	0.89 ± 0.42	0.88 ± 0.39	1.09 ± 0.38
3 corner lights off	0.94 ± 0.42	1.03 ± 0.36	1.21 ± 0.54

Line of Sight Obstruction

Table 20: Detection Rates for Marker Obstruction

	Marker ID 0	Marker ID 10	Marker ID 20	Marker ID 30	Marker ID 40
0 bits	100%	100%	100%	100%	100%
0.5 bits	12.5%	16.67%	12.5%	12.5%	16.67%
1 bit	0%	0%	0%	0%	0%
1.5 bits	0%	0%	0%	0%	0%

5.3 Discussion

The results indicate that of the operating room and camera parameters, line-of-sight obstruction (Table 20) affected tracking the most. This makes sense because of the low pixel density that ArUco codes have compared to QR codes - most of the ArUco pixels are dedicated towards helping make detection easier and tracking more accurate. This meant that even a 0.5 bit obstruction would drastically decrease the ArUco detection rate and make them unusable for tracking in the interventional pain management therapies. TCS Research and Innovation devised a way to give ArUco codes error correction using border segments and Reed-Solomon codes [76]. But if their work is to be included with future skin markers, the subsequent increased pixel density will have to be accounted for.

Other variables that influenced tracking accuracy were camera distance (Table 15) and marker border (Table 11). The camera distance tests showed an approximate decrease of 24.1% in the error from 60 cm to 50 cm. The white code border serves to provide a strong contrast to help detect the edges of the code. When the border was decreased, the contrast also decreased which then led to the drastic drop in detection rate.

Surprisingly, the 6x6 and 7x7 pixel markers were rarely detected (Table 9). This could be due to the specific camera used or perhaps the markers needing more than a 1 bit border for detection. Another surprise was the marker size error (Table 10), which seemed to correlate to marker size. However, it should be noted that the supposed best case scenario of 2 cm markers had a 99.95% detection rate rather than 100%.

There were also rare occasions where the tracking algorithm saw false positive ArUco codes. The most mistaken codes were 17, 37, and 85, with markers 17 and 37 being by far the most common error.

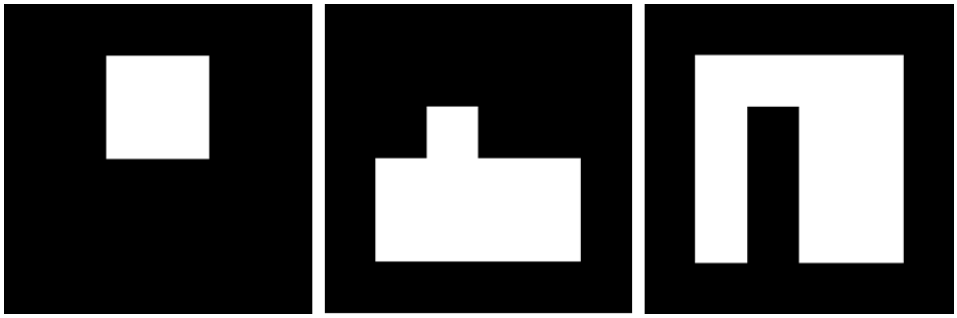

Figure 22: ArUco 4x4 Markers 17, 37, and 85 respectively

As seen in Figure 22, the patterns of marker IDs 17, 37, and 85 are not very complex. This increases the likelihood of a random object or shading tricking the code into seeing a false positive marker. While these codes were filtered out during the MATLAB data processing, future studies should try to decrease or even eliminate the false positive detection rate.

The variables that can likely be manipulated to ensure better accuracy are the marker properties (pixel density, marker size, marker border, and marker contrast) and the camera resolution and frames per second settings. If these variables are adjusted according to the context of the patient and procedure, then the number of potential factors in the operating room that could affect tracking would decrease.

However, variables such as the operating room conditions, marker warping, and camera placement may be more difficult to control. There are also other variables that have yet to be tested such as those relating to the patient: skin movements, sweating, showering, scratching, house room temperature, etc. All of these variables could result in inconsistencies with unpredictable effects between each procedure.

All of the mentioned experiments tested ArUco codes that were printed on paper. However, an actual skin marker would most likely be made from different materials, the tracking properties of which may be influenced very differently under the same operating room conditions compared to paper marker tracking. While many tests were conducted, there are still other parameters to be

considered and tested in the future to see how they affect tracking. Since the markers are intended to be attached to the patient's skin for up to two weeks, there is potential for the markers to get damaged during that time. There is also a need to find the right balance between the most accurate marker and the patient. For example, an increase in marker size could lead to increased tracking accuracy but may be more susceptible to damage due to the increased area.

Lastly, it should be noted that each variable tested is not independent of each other (ie. marker size and camera distance). In the actual operating room, many variables are present and may interact with each other, affecting the accuracy of tracking. It is important to conduct multi-variable and dynamic experiments in the future in order to better simulate the in-situ interventional pain management therapy procedures. A comprehensive study of all the variables and their interdependencies will help a physician better understand which skin markers are best suited for a patient given the patient's lifestyle and habits and the operating room conditions.

Overall, the mean error and standard deviation of the default parameters was 0.88 ± 0.40 mm. This is just the start with only one camera and a basic tracking algorithm. It is expected that both the camera setup and the tracking algorithm will become more advanced as the project progresses to further decrease the skin marker errors.

Chapter 6 Conclusion and Future Directions

6.1 Conclusion

The experiments conducted during the duration of this study showed promising results and future directions to an affordable navigation system for pain management. In consideration for future research and development, three key takeaways should be considered for the non-invasive pain management system.

- If a method can be found to analyze the errors of the platform more quickly, then the XYZ platform can be quickly reanalyzed to determine the actual undershoot of the motors and retuned. Also, after reducing the tolerance of the Z axis's rack and pinion mechanism, the XYZ platform can be depended upon to simulate a patient's body movements.
- The mean error and standard deviation of the default parameters was 0.88 ± 0.40 mm. Since not all of these parameters used the most optimal settings, there is the opportunity to further reduce the tracking error. However, for non-optimal parameters such as a 70 cm camera distance, the marker error may exceed one millimeter. Therefore, it is important to know how each parameter affects the tracking accuracy and then manipulate those parameters to reduce the tracking error.
- If the tracking error can be decreased even further and the marker is viable for interventional pain management therapies, then the overall system will be considerably cheaper than the surgical systems mentioned in Chapter 1 which cost over $470,000. The costs of the markers and cameras are relatively cheap, and most of the costs would come from the MRI scanning and the augmented reality software.

6.2 Future Directions

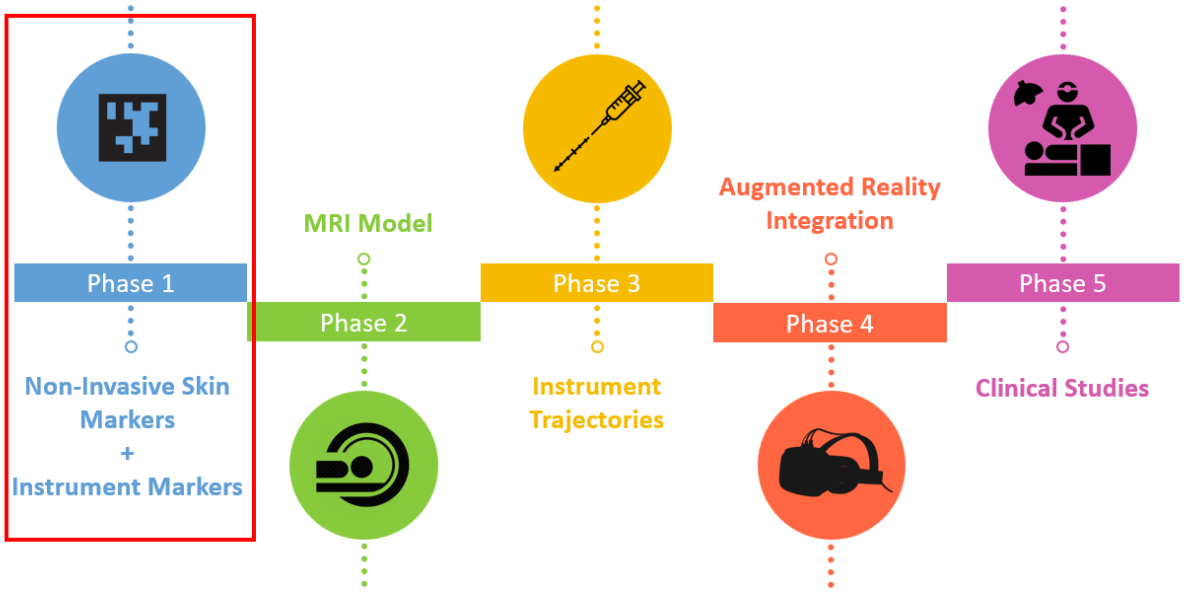

Figure 23: Current Progress in Project Phases

The work done in this thesis is part of Phase 1 of the proposed 3D augmented reality navigation system. However, as it is the first step, there are many aspects of the project that need to be developed if this project is to be successful.

6.2.1 Short-Term Future

Marker Placement on the Skin

Skin markers are a reliable method of surface tracking, but their reliability diminishes if the procedure point is further within the body. There are two main types of errors that need to be taken into consideration with skin markers: fiducial registration error (FRE) and tracking registration error (TRE). FRE refers to the error of the skin markers on the patient and the corresponding points on a CT or MRI image while TRE refers to the error at the target point within the body [77]. Fiducial recognition error is more often used as the error of registration since tracking recognition error is within the patient's body and therefore more difficult to measure.

However, as shown in Figure 23, small fiducial recognition error does not represent small tracking recognition error.

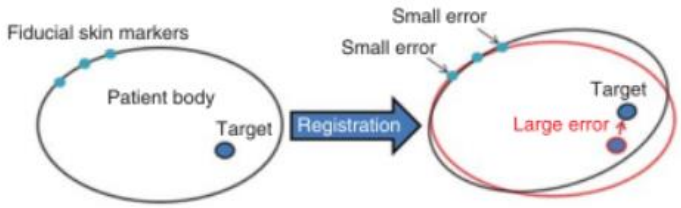

Figure 24: Small FRE can still lead to large TRE [77]

It was found that the placement of markers can greatly influence tracking registration error [78] and therefore it is important to not only find the optimal positions for reducing the tracking registration error, but also ensure the skin markers can last on the patient's skin for up to two weeks.

Marker Materials

Since the skin markers are needed to last on the patient's skin for up to two weeks until the procedure, extensive testing will be needed to determine the optimal marker materials for the patient. Such tests can involve biocompatibility (to ensure the material is safe for the patient), peel (to test how easily the marker can accidentally be removed), durability (to see whether the markers are still clearly visible and can be accurately tracked), and breathability (to make sure that the markers are not affected by perspiration). The skin markers should also account for the skin's anisotropic properties.

Marker Shifting

It is important to devise a method to detect whether the markers shifted, peeled, or have been replaced on the patient. Even though having a marker fall off is bad, it is potentially more dangerous if the marker is restuck by the patient in a different location. The difference in marker

location will cause the augmented reality overlay to be inaccurate and could potentially lead to severe consequences during the procedure [79].

Instrument Marker Platform

Both the non-invasive skin markers and instruments need to be tracked throughout the procedure in order for the navigation system to work. As such, an instrument platform that can mimic the needle movements during a procedure needs to be built. The instrument platform is planned to be built such that it can operate in conjunction with the XYZ platform to simulate both the patient and the needles at the same time to better simulate operating room conditions.

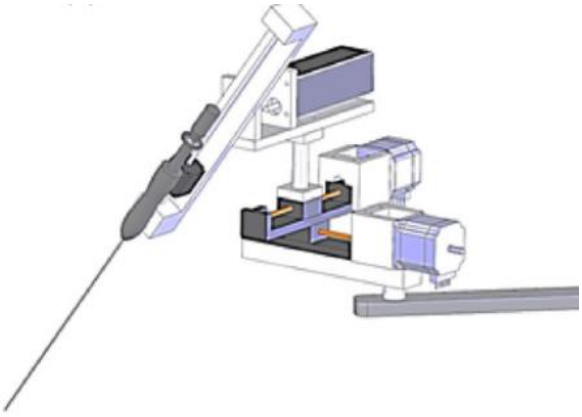

Figure 25: An example of a needle insertion platform [80]

Improved Camera Setup and Live Tracking

The current camera setup only utilizes one camera for simplicity but it results in a lack of depth perception for the computer vision algorithm. A multi-camera setup will be explored during the summer of 2022.

The current experiments analyze video recordings rather than live streams. However, it should be noted that the higher the resolution and frame rate of the videos, the more information needs to be processed by the algorithm which could result in delays. There needs to be a balance between the processing speed of the algorithm and the accuracy of the tracking.

6.2.2 Long-Term Future

MRI Model

Even though the MRI scans create a very detailed model of the patient's body, it should be noted that the patient will most likely be in a different position during the operation compared to during the MRI scan. Therefore, the MRI model will need to be adaptable to the patient's body positions and breathing patterns. Also, if the augmented reality MRI model contains too much information, the physician should be given an option to adjust the MRI model to their preference. Such options may include cropping the MRI model, adjusting transparencies, or removing certain organs and structures within the body.

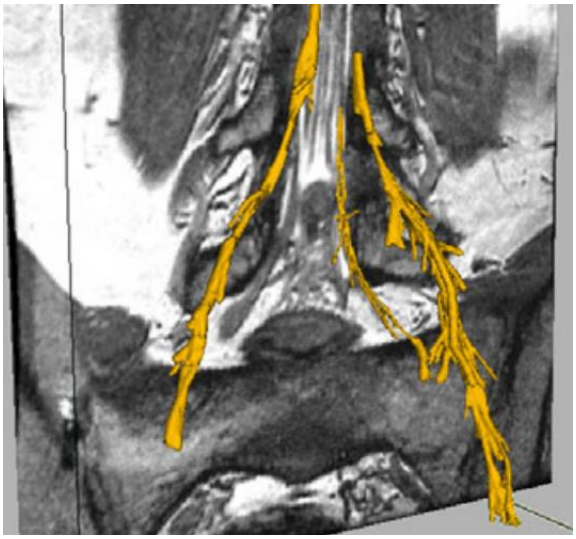

Figure 26: MRI model that segmented the hip nerve bundles for easier visualization [81]

Instrument Trajectories

The advantage of having a preoperative scan is that the physician can carefully plan out the procedure in advance. This is particularly helpful when the patient has spine degeneration or deformations that make it more difficult to precisely insert the needle. To supplement the physicians, especially newer physicians, machine learning algorithms can be developed to suggest

optimal needle trajectories for each patient but still allow for adjustments based on physician preferences.

Augmented Reality Integration

Once all of the above projects are completed, then they can be integrated together into augmented reality. This would be particularly helpful in allowing physicians to keep their full focus on the patient in front of them and to see both the patient's 3D anatomy and the suggested instrument trajectory instead of needing to look at external monitors.

Clinical Trials and Expansion to Other Procedures

Comprehensive testing can begin with surgical dummies, continue with cadavers, and then finally to clinical trials for epidural steroid injections and radiofrequency ablations. If the augmented reality navigation system is proven to be effective in interventional pain therapies, then it can be expanded to different procedures such as knee implants.

Appendix

The following Appendix Figures A1-13 visualize the tracking coordinates and errors of the tracking algorithm. In each figure, the left column shows the tracking coordinates as seen by the camera and calculated by the tracking algorithm while the right column shows a heatmap of the tracking errors relative to the programmed XYZ platform pattern.

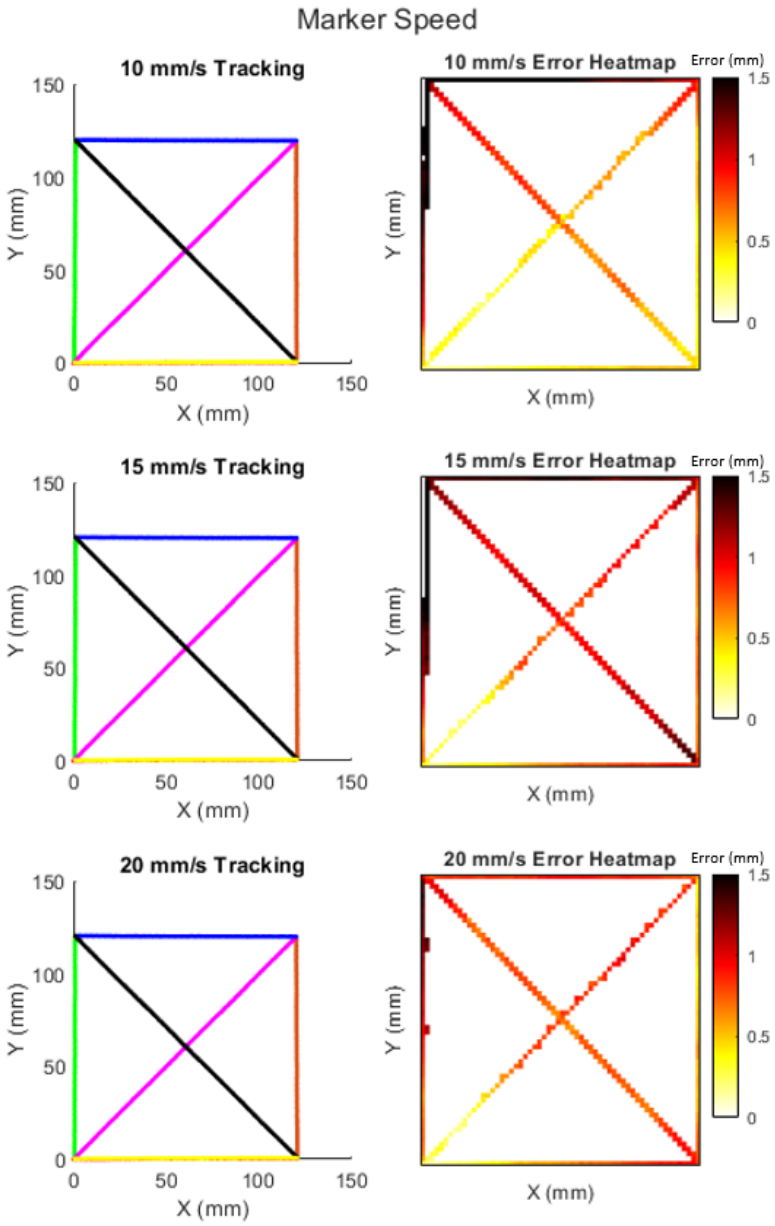

Figure A1: Data Visualization of Marker Speeds of 10, 15, and 20 mm/s

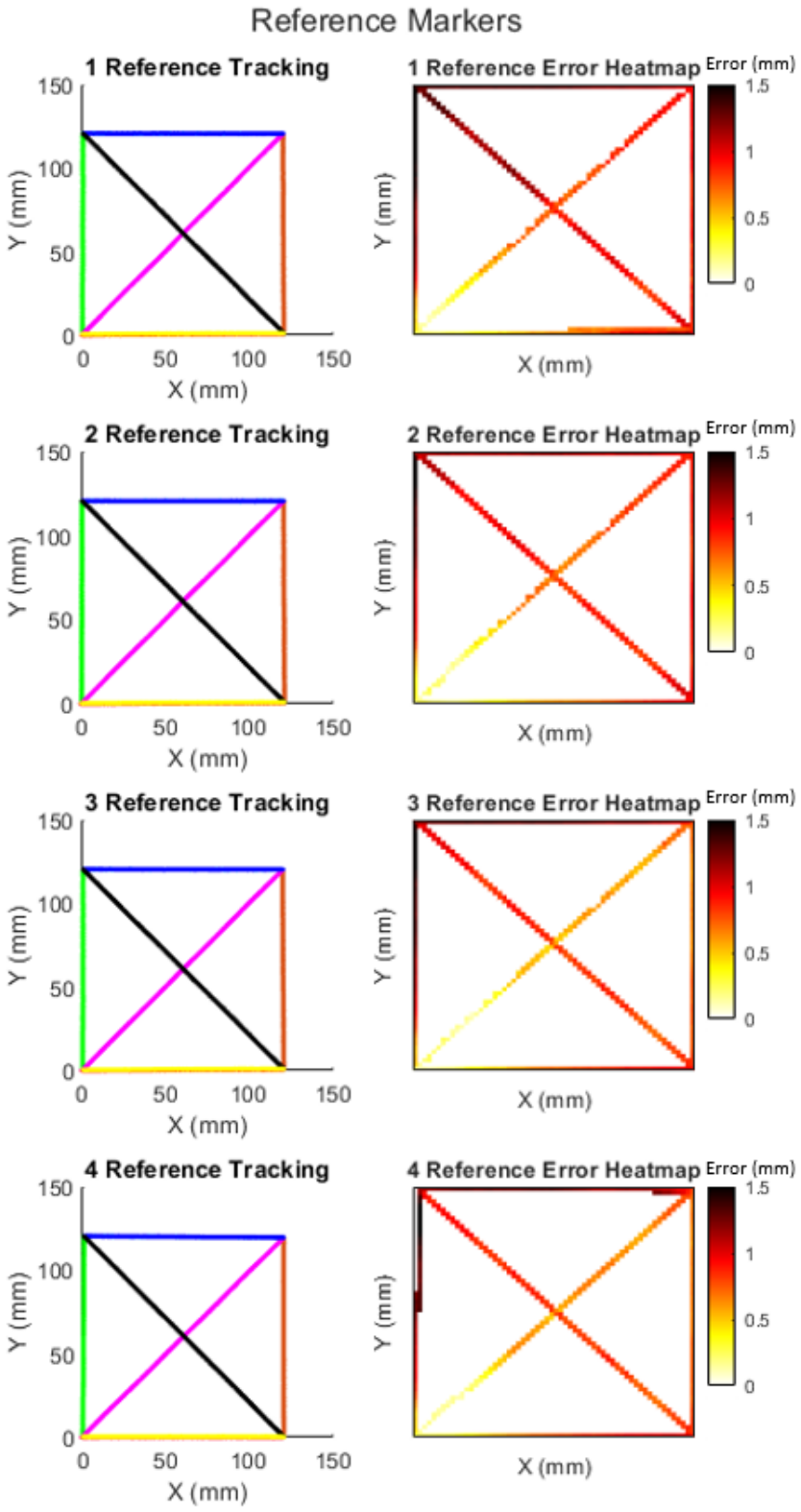

Figure A2: Data Visualization of 1, 2, 3, and 4 Reference Markers

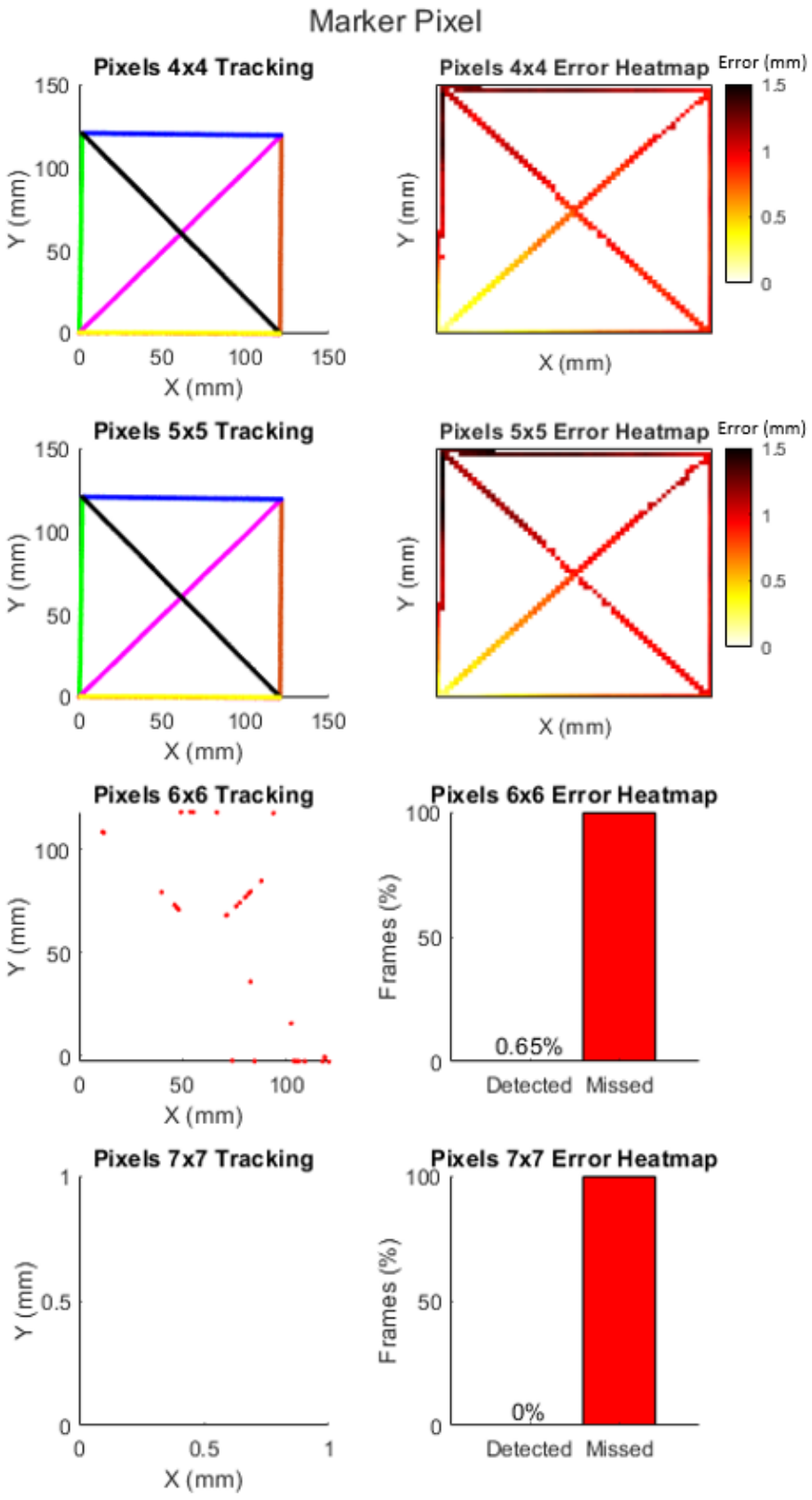

Figure A3: Data Visualization of 4x4, 5x5, 6x6, and 7x7 Pixel Densities

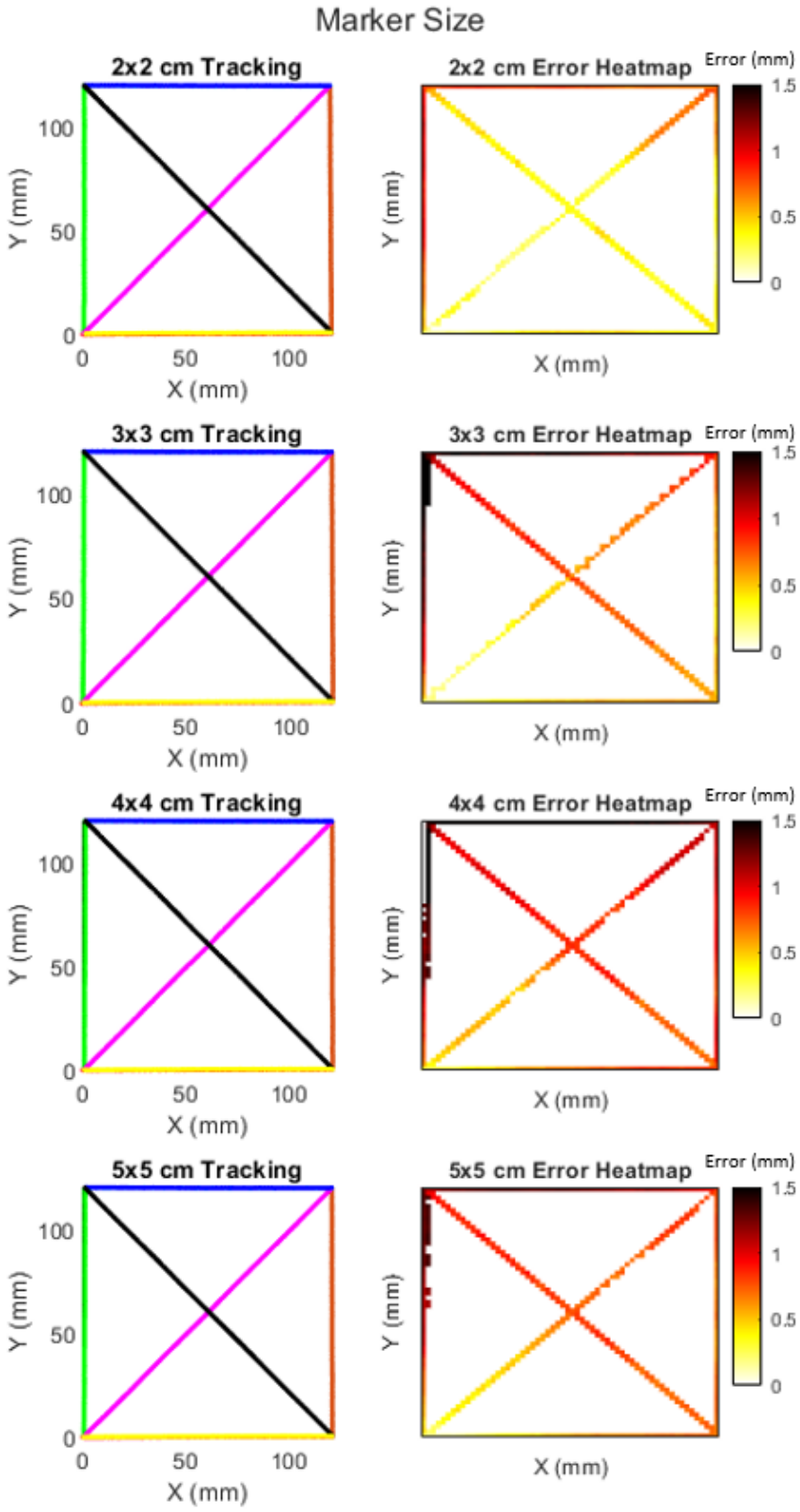

Figure A4: Data Visualization of 2x2, 3x3, 4x4, and 5x5 cm Marker Sizes

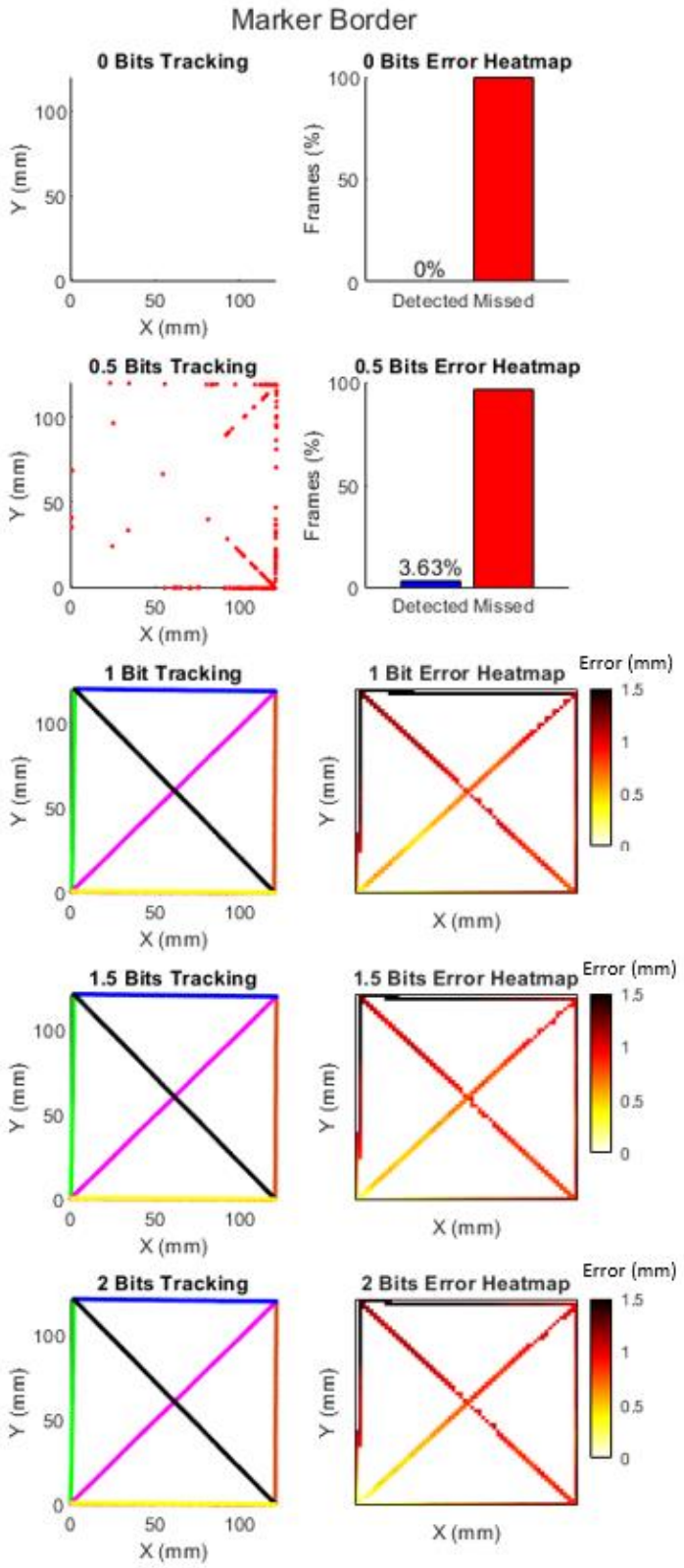

Figure A5: Data Visualization of 0, 0.5, 1, 1.5, and 2 Bit Marker Borders

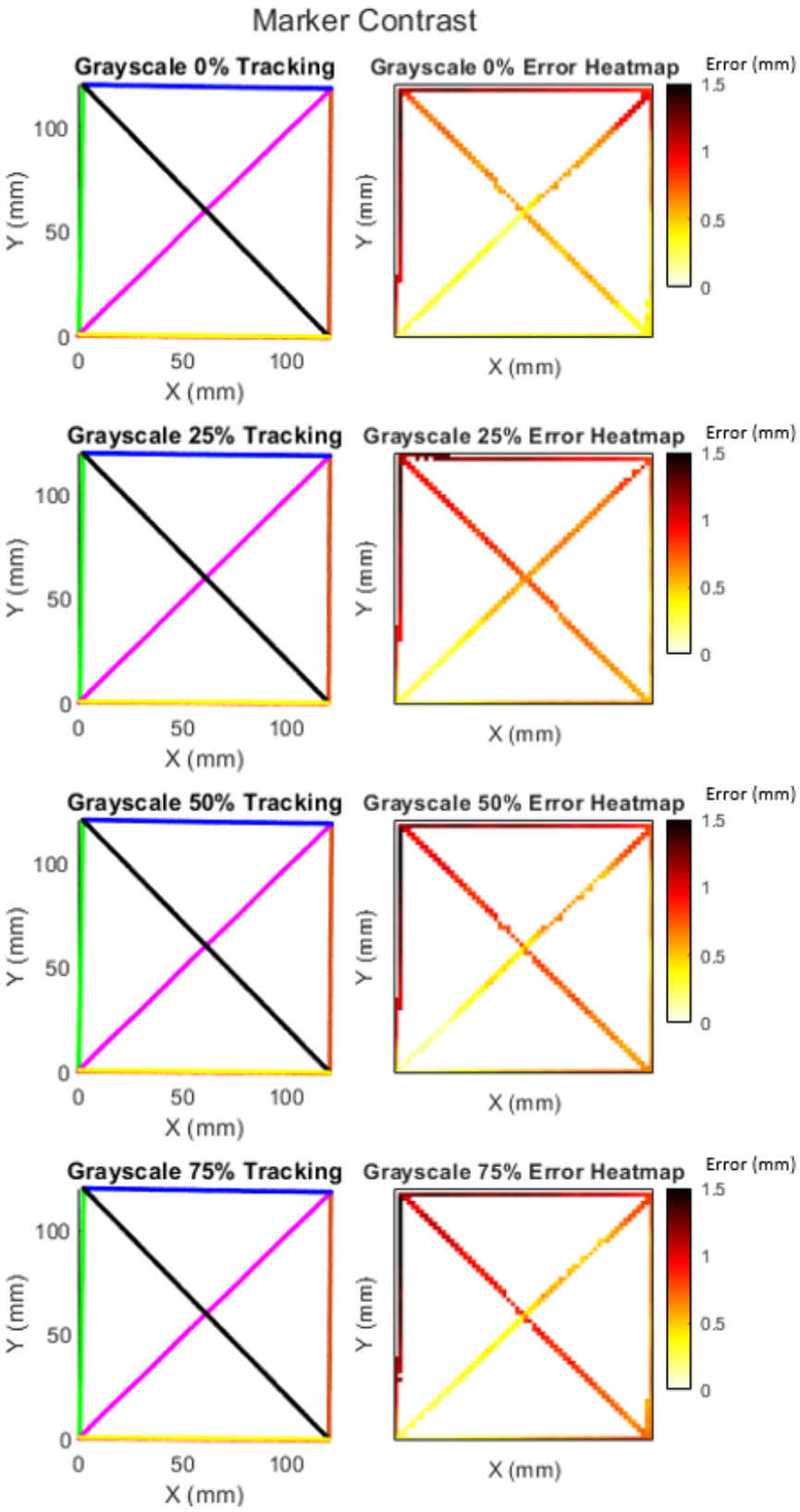

Figure A6: Data Visualization of 0, 25, 50, and 75% Grayscale Marker Contrasts

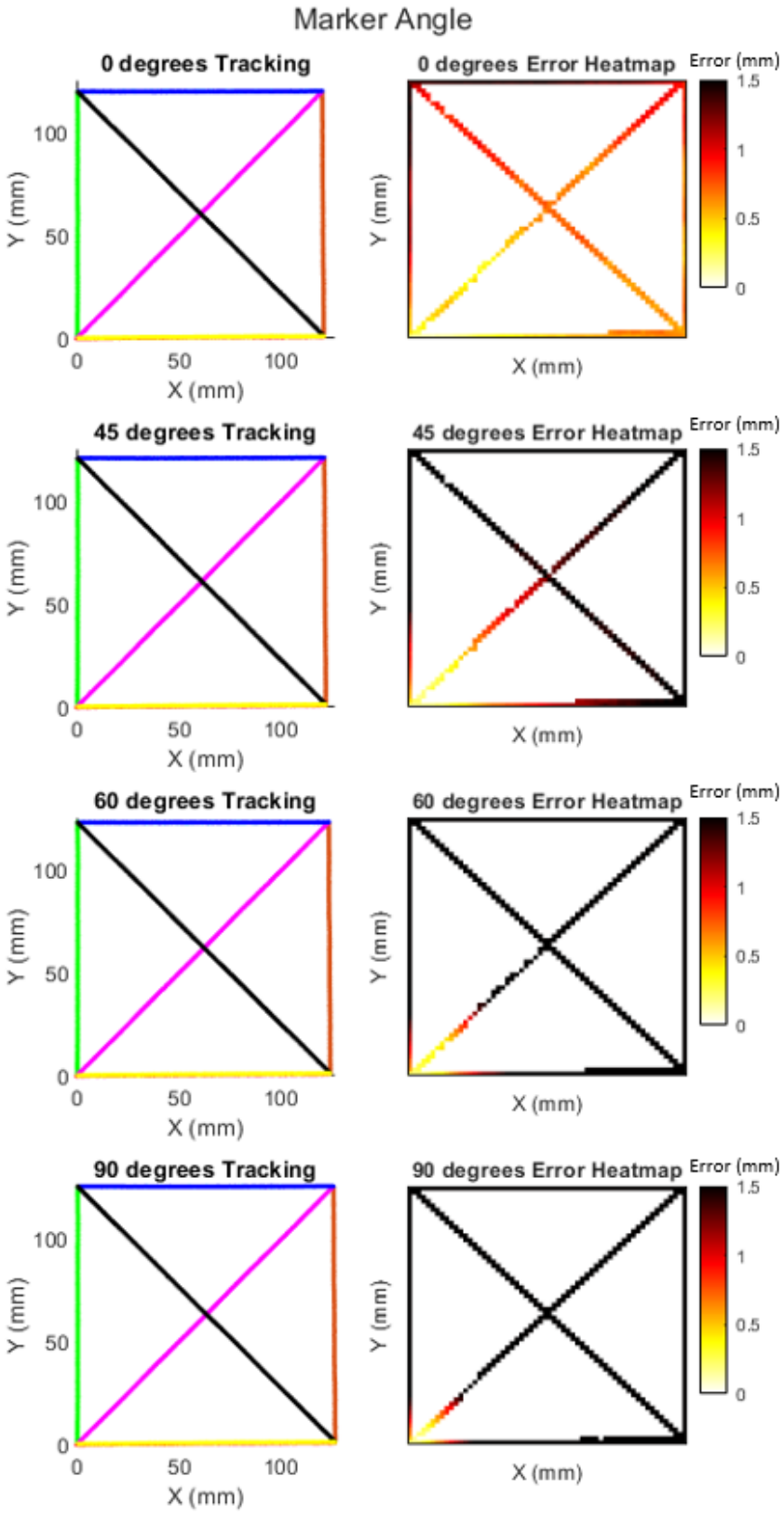

Figure A7: Data Visualization of 0, 45, 60, and 90 degree Marker Angles

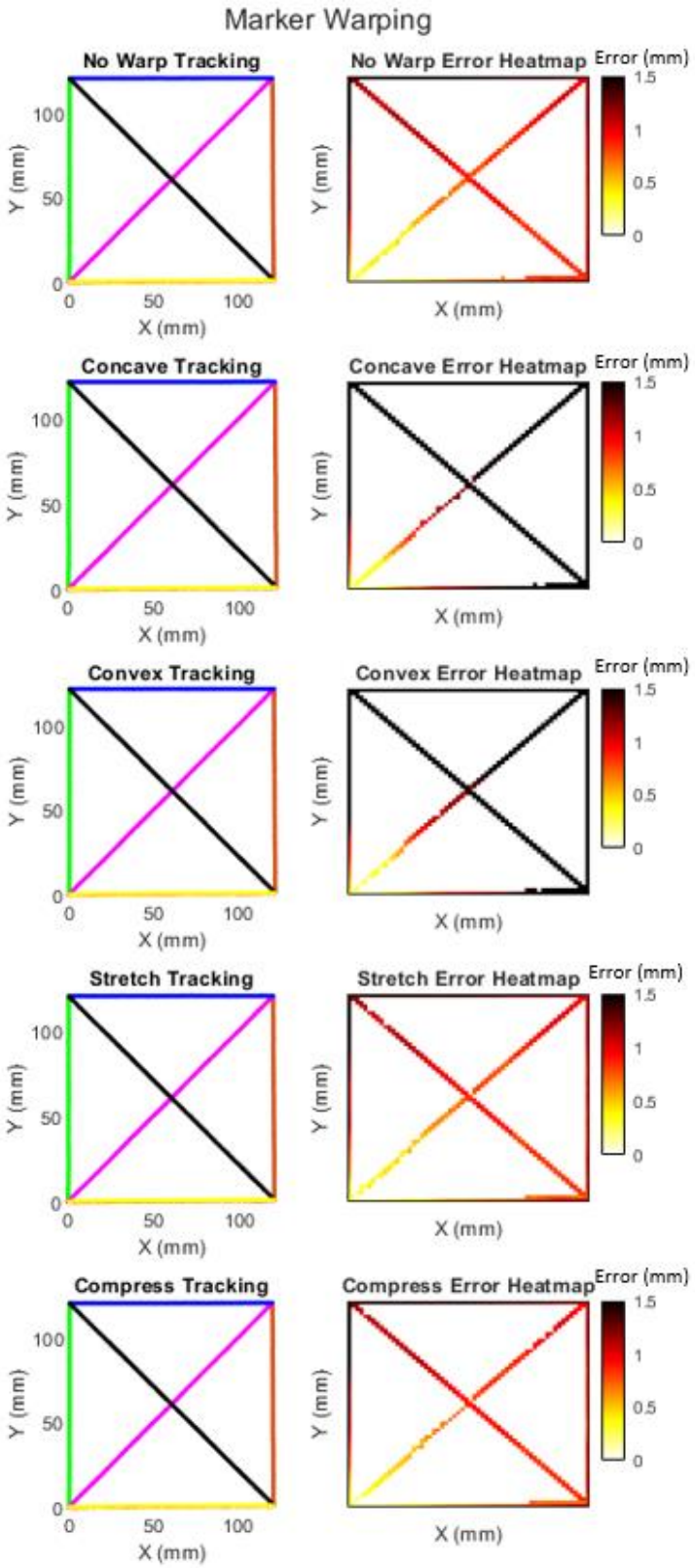

Figure A8: Data Visualization of Marker Warping: Concave, Convex, Stretch, and Compress

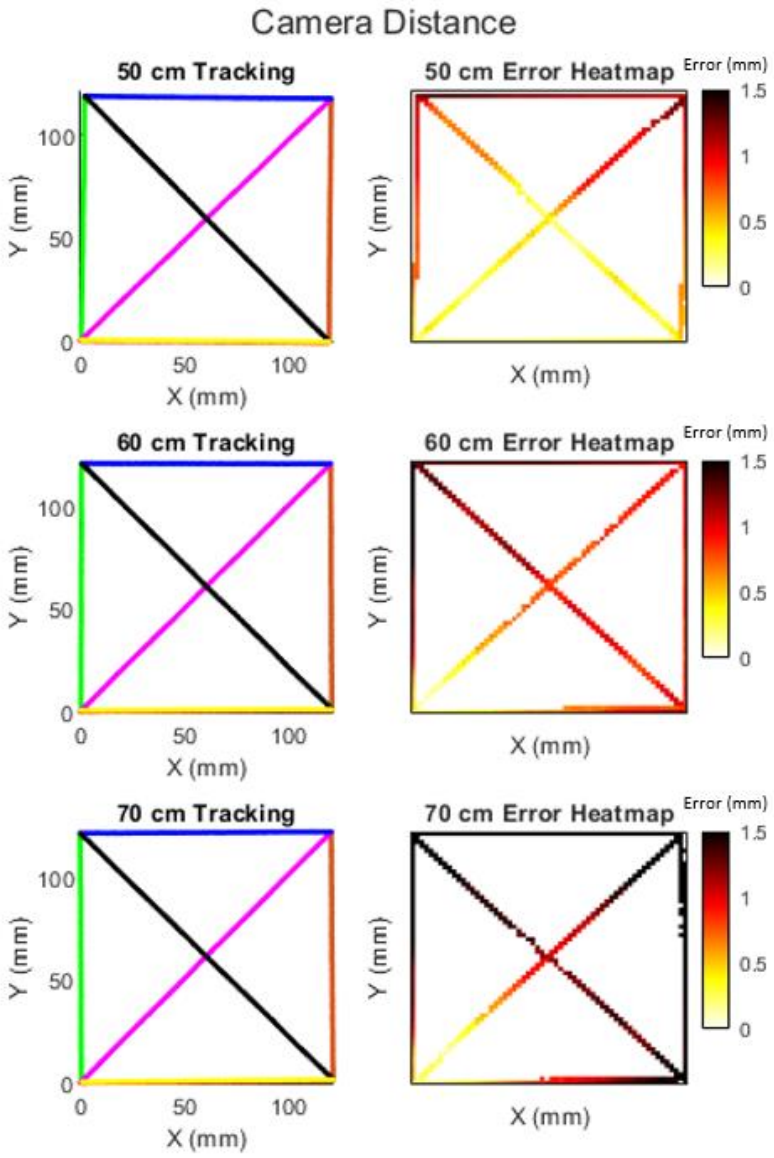

Figure A9: Data Visualization of 50, 60, and 70 cm Camera Distances

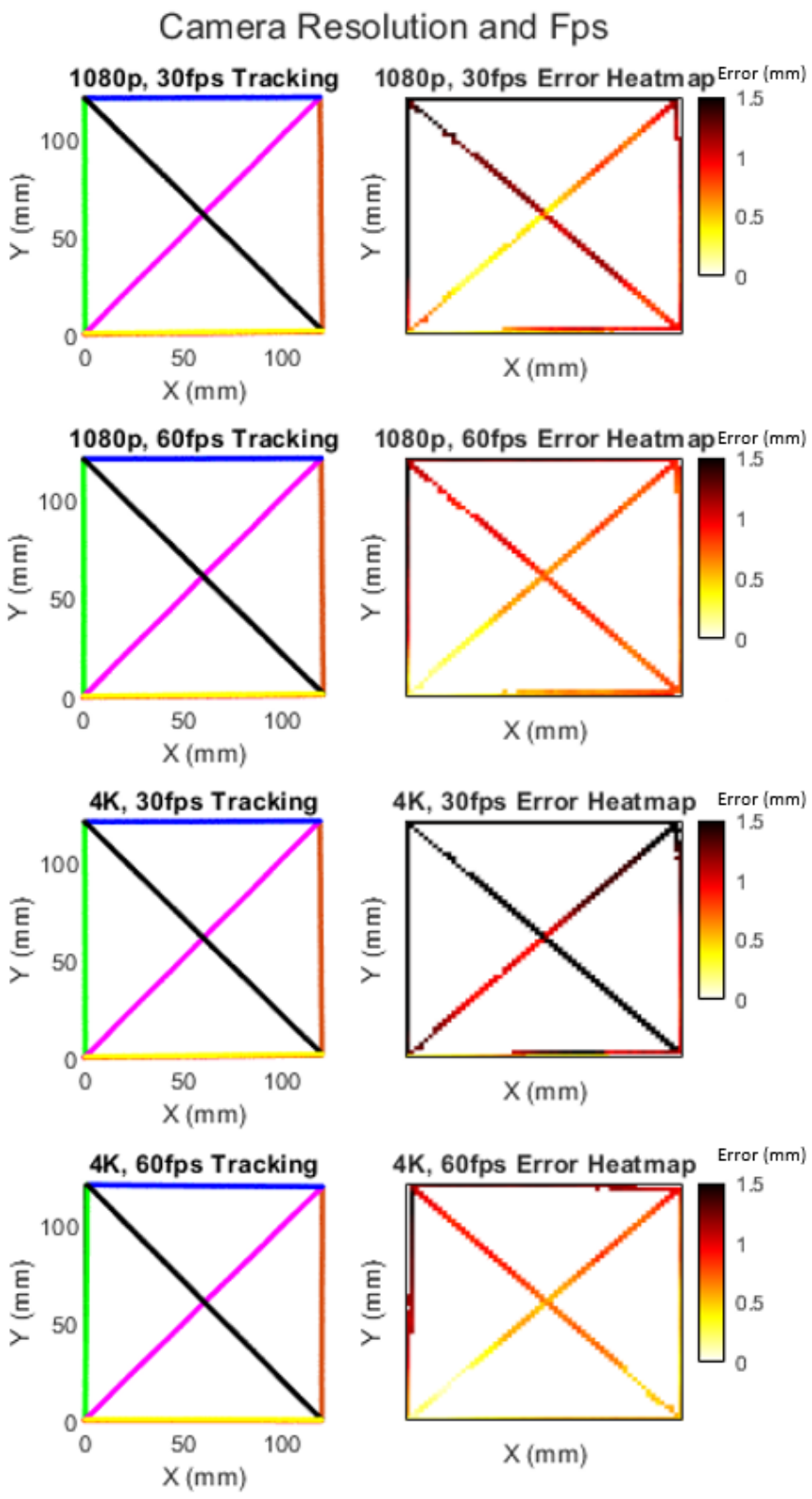

Figure A10: Data Visualization of 1080p and 4K Camera Resolution, and 30 and 60 Frames per Second

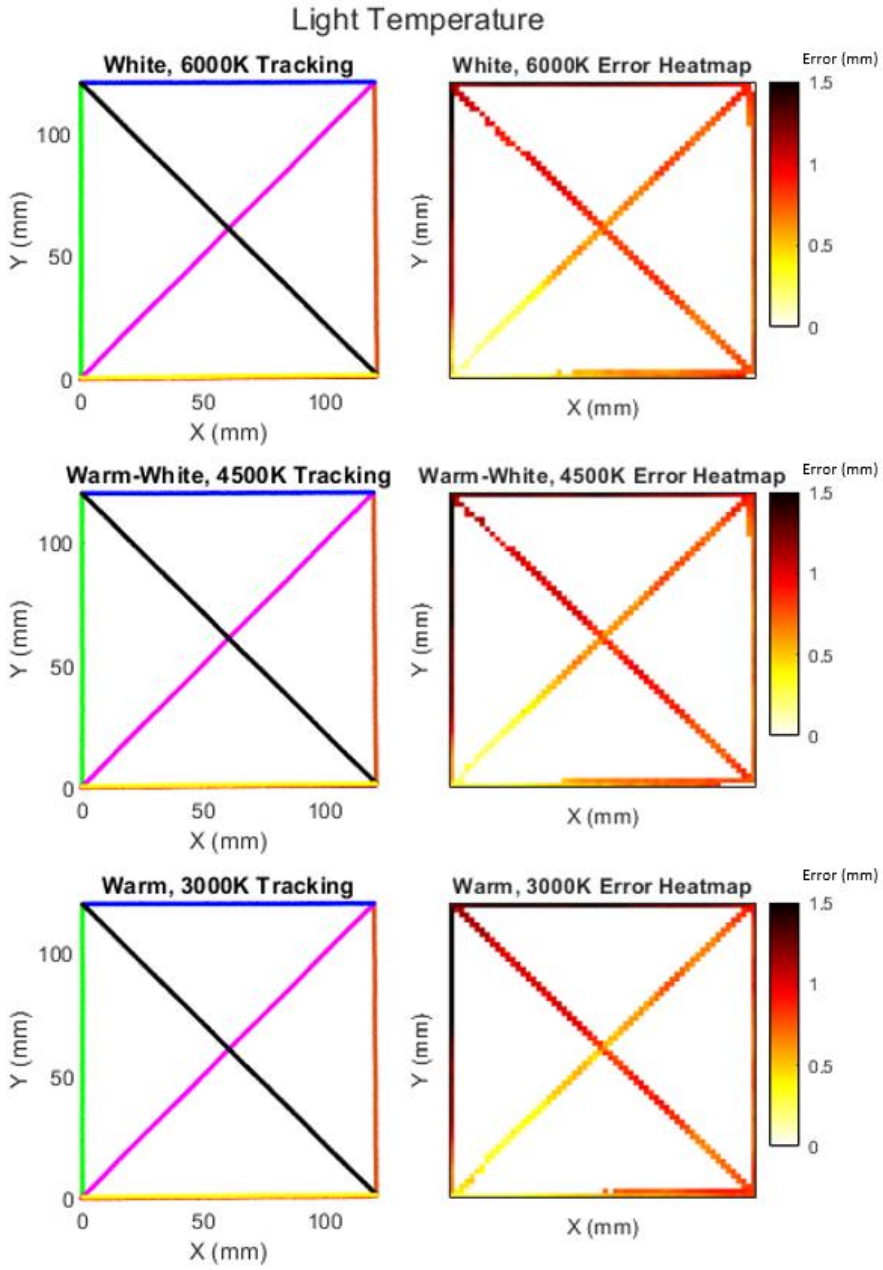

Figure A11: Data Visualization of 6000, 4500, and 3000K Light Temperature

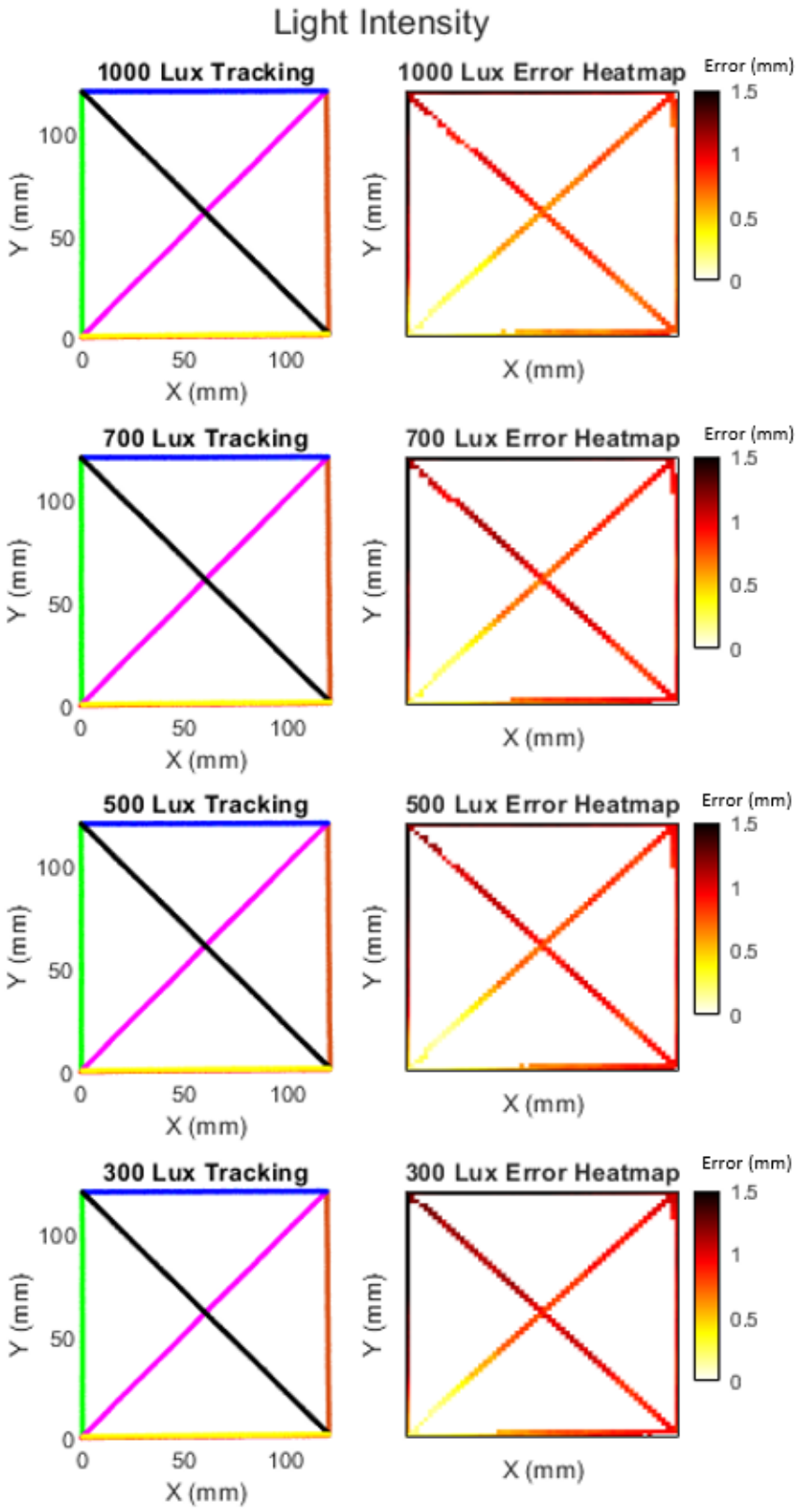

Figure A12: Data Visualization of 1000, 700, 500, and 300 Lux in Light Intensity

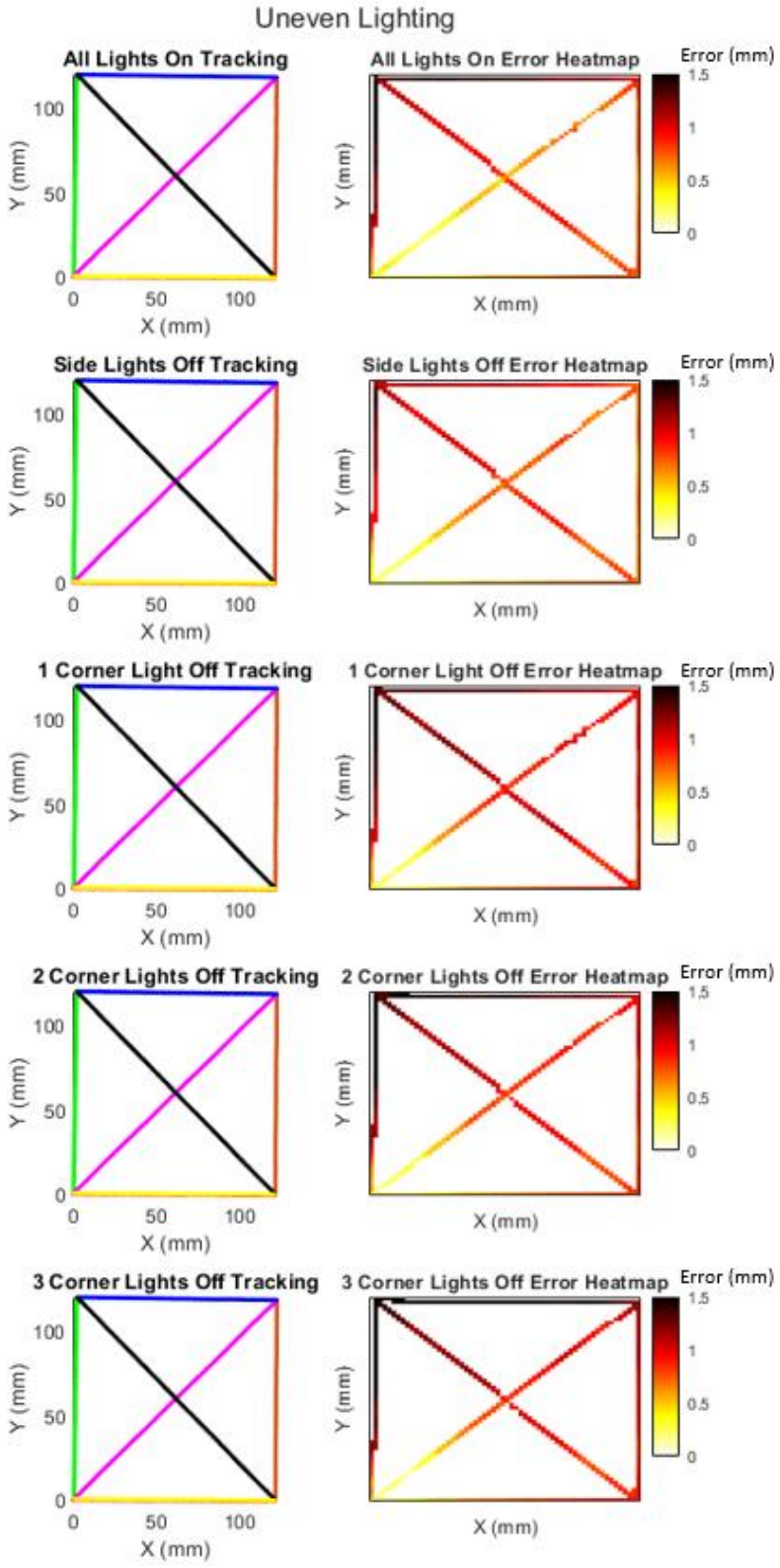

Figure A13: Data Visualization of Uneven Lighting as Lamps Around the Perimeter are Turned Off

References

[1] S. L. James et al., *Global, Regional, and National Incidence, Prevalence, and Years Lived with Disability for 354 Diseases and Injuries for 195 Countries and Territories, 1990–2017: A Systematic Analysis for the Global Burden of Disease Study 2017*, The Lancet **392**, 1789 (2018).

[2] L. Manchikanti, V. Singh, F. J. E. Falco, R. M. Benyamin, and J. A. Hirsch, *Epidemiology of Low Back Pain in Adults*, Neuromodulation Technol. Neural Interface **17**, 3 (2014).

[3] P. S. Sizer, O. Matthijs, and V. Phelps, *Influence of Age on the Development of Pathology*, Curr. Rev. Pain **4**, 362 (2000).

[4] M. C. Battié, T. Videman, L. E. Gibbons, L. D. Fisher, H. Manninen, and K. Gill, *1995 Volvo Award in Clinical Sciences. Determinants of Lumbar Disc Degeneration. A Study Relating Lifetime Exposures and Magnetic Resonance Imaging Findings in Identical Twins*, Spine **20**, 2601 (1995).

[5] F. Kovacs, J. Noguera, V. Abraira, A. Royuela, A. Cano, M. Gel del Real, J. Zamora, M. Gestoso, A. Muriel, N. Mufraggi., *The Influence of Psychological Factors on Low Back Pain-Related Disability in Community Dwelling Older Persons*, Pain Med. **9**, 871 (2008).

[6] P. R. Croft, A. C. Papageorgiou, S. Ferry, E. Thomas, M. I. Jayson, and A. J. Silman, *Psychologic Distress and Low Back Pain. Evidence from a Prospective Study in the General Population*, Spine **20**, 2731 (1995).

[7] M. Truchon, D. Côté, L. Fillion, B. Arsenault, and C. Dionne, *Low-Back-Pain Related Disability: An Integration of Psychological Risk Factors into the Stress Process Model*, Pain **137**, 564 (2008).

[8] S. R. Currie and J. Wang, *More Data on Major Depression as an Antecedent Risk Factor for First Onset of Chronic Back Pain*, Psychol. Med. **35**, 1275 (2005).

[9] J. Walker, B. Sofaer, and I. Holloway, *The Experience of Chronic Back Pain: Accounts of Loss in Those Seeking Help from Pain Clinics*, Eur. J. Pain **10**, 199 (2006).

[10] B. I. Martin, *Expenditures and Health Status Among Adults With Back and Neck Problems*, JAMA **299**, 656 (2008).

[11] E. A. Shipton, *Physical Therapy Approaches in the Treatment of Low Back Pain*, Pain Ther. **7**, 127 (2018).

[12] M. Almeida, B. Saragiotto, B. Richards, and C. G. Maher, *Primary Care Management of Non-specific Low Back Pain: Key Messages from Recent Clinical Guidelines*, Med. J. Aust. **208**, 272 (2018).

[13] A. C. Gellhorn, L. Chan, B. Martin, and J. Friedly, *Management Patterns in Acute Low Back Pain: The Role of Physical Therapy*, Spine **37**, 775 (2012).

[14] J. M. A. Mens, *The Use of Medication in Low Back Pain*, Best Pract. Res. Clin. Rheumatol. **19**, 609 (2005).

[15] D. C. Cherkin, K. J. Wheeler, W. Barlow, and R. A. Deyo, *Medication Use for Low Back Pain in Primary Care:*, Spine **23**, 607 (1998).

[16] A. Y. Wong, J. Karppinen, and D. Samartzis, *Low Back Pain in Older Adults: Risk Factors, Management Options and Future Directions*, Scoliosis Spinal Disord. **12**, 14 (2017).

[17] J. N. A. Gibson and G. Waddell, *Surgical Interventions for Lumbar Disc Prolapse: Updated Cochrane Review*, Spine **32**, 1735 (2007).

[18] J. N. A. Gibson and G. Waddell, *Surgery for Degenerative Lumbar Spondylosis: Updated Cochrane Review*, Spine **30**, 2312 (2005).

[19] B. Morlion, *Chronic Low Back Pain: Pharmacological, Interventional and Surgical Strategies*, Nat. Rev. Neurol. **9**, 462 (2013).

[20] M. W. van Tulder, B. Koes, S. Seitsalo, and A. Malmivaara, *Outcome of Invasive Treatment Modalities on Back Pain and Sciatica: An Evidence-Based Review*, Eur. Spine J. **15**, S82 (2006).

[21] A. G. MD, *Cervical Epidural Steroid Injections Can Bring Neck and Arm Pain Relief*, https://www.spine-health.com/blog/visual-guide-cervical-epidural-steroid-injections.

[22] N. R. Abraham, I. Badiola, and T. D. Vo, *Epidural (Cervical, Thoracic, Lumbar, Caudal) Block/Injections*, in *Comprehensive Treatment of Chronic Pain by Medical, Interventional, and Integrative Approaches*, edited by T. R. Deer, M. S. Leong, A. Buvanendran, V. Gordin, P. S. Kim, S. J. Panchal, and A. L. Ray (Springer New York, New York, NY, 2013), pp. 359–366.

[23] M. Araujo and D. M. O'Ferrall, *Complications of Interventional Pain Management Techniques*, in *Comprehensive Treatment of Chronic Pain by Medical, Interventional, and Integrative Approaches*, edited by T. R. Deer, M. S. Leong, A. Buvanendran, V. Gordin, P. S. Kim, S. J. Panchal, and A. L. Ray (Springer New York, New York, NY, 2013), pp. 727–741.

[24] *What You Should Know About Epidural Steroid Injections | HSS*, https://www.hss.edu/conditions_epidural-injections-faqs.asp.

[25] R. B. MD, *Cervical, Thoracic and Lumbar Interlaminar Epidural Injections*, https://www.spine-health.com/treatment/injections/cervical-thoracic-and-lumbar-interlaminar-epidural-injections.

[26] *Radiofrequency Ablation*, https://healthykcmag.com/radiofrequency-ablation/.

[27] M. V. Rana, *Radiofrequency: Conventional and Pulsed*, in *Comprehensive Treatment of Chronic Pain by Medical, Interventional, and Integrative Approaches*, edited by T. R. Deer, M. S. Leong, A. Buvanendran, V. Gordin, P. S. Kim, S. J. Panchal, and A. L. Ray (Springer New York, New York, NY, 2013), pp. 285–296.

[28] D. K. MD, *Radiofrequency Ablation (RFA) for Facet and Sacroiliac Joint Pain*, https://www.spine-health.com/treatment/injections/radiofrequency-ablation-rfa-facet-and-sacroiliac-joint-pain.

[29] F. J. Yuk, G. A. Maragkos, K. Sato, and J. Steinberger, *Current Innovation in Virtual and Augmented Reality in Spine Surgery*, Ann. Transl. Med. **9**, 94 (2021).

[30] T. J. Brigham, *Reality Check: Basics of Augmented, Virtual, and Mixed Reality*, Med. Ref. Serv. Q. **36**, 171 (2017).

[31] J. S. Yoo, D. S. Patel, N. M. Hrynewycz, T. S. Brundage, and K. Singh, *The Utility of Virtual Reality and Augmented Reality in Spine Surgery*, Ann. Transl. Med. **7**, S171 (2019).

[32] J. H. Shuhaiber, *Augmented Reality in Surgery*, Arch. Surg. **139**, 170 (2004).

[33] P. Vávra, J. Roman, P. Zonča, P. Ihnát, M. Němec, J. Kumar, N. Habib, and A. El-Gendi, *Recent Development of Augmented Reality in Surgery: A Review*, J. Healthc. Eng. **2017**, 1 (2017).

[34] G. Burström, O. Persson, E. Edström, and A. Elmi-Terander, *Augmented Reality Navigation in Spine Surgery: A Systematic Review*, Acta Neurochir. (Wien) **163**, 843 (2021).

[35] H. Liu, J. Wu, Y. Tang, H. Li, W. Wang, C. Li, and Y. Zhou, *Percutaneous Placement of Lumbar Pedicle Screws via Intraoperative CT Image–Based Augmented Reality–Guided Technology*, J. Neurosurg. Spine **32**, 542 (2020).

[36] C. Dennler, L. Jaberg, J. Spirig, C. Agten, T. Götschi, P. Fürnstahl, and M. Farshad, *Augmented Reality-Based Navigation Increases Precision of Pedicle Screw Insertion*, J. Orthop. Surg. **15**, 174 (2020).

[37] Z. Zhou, Z. Yang, S. Jiang, F. Zhang, and H. Yan, *Design and Validation of a Surgical Navigation System for Brachytherapy Based on Mixed Reality*, Med. Phys. **46**, 3709 (2019).

[38] J. Driver and M. W. Groff, *Editorial. Navigation in Spine Surgery: An Innovation Here to Stay*, J. Neurosurg. Spine **36**, 347 (2022).

[39] A. Liu, J. Yike, C. Ethan, K. Majid, W. Erick, E. Jeff, P. Zach, L. Sheng-fu, S. Daniel, M. Camilo, W. Timothy., *Clinical Accuracy and Initial Experience with Augmented Reality–Assisted Pedicle Screw Placement: The First 205 Screws*, J. Neurosurg. Spine **36**, 351 (2021).

[40] C. A. Molina, D. M. Sciubba, J. K. Greenberg, M. Khan, and T. Witham, *Clinical Accuracy, Technical Precision, and Workflow of the First in Human Use of an Augmented-Reality Head-Mounted Display Stereotactic Navigation System for Spine Surgery*, Oper. Neurosurg. **20**, 300 (2021).

[41] *ClarifEye Augmented Reality Surgical Navigation*, https://www.philips.com/a-w/about/news/media-library/20210202-clarifeye-augmented-reality-surgical-navigation.html.

[42] P. Auloge, R. L. Cazzato, N. Ramamurthy, P. de Marini, C. Rousseau, J. Garnon, Y. P. Charles, J.-P. Steib, and A. Gangi, *Augmented Reality and Artificial Intelligence-Based Navigation during Percutaneous Vertebroplasty: A Pilot Randomised Clinical Trial*, Eur. Spine J. **29**, 1580 (2020).

[43] E. Edström, G. Burström, R. Nachabe, P. Gerdhem, and A. Elmi Terander, *A Novel Augmented-Reality-Based Surgical Navigation System for Spine Surgery in a Hybrid Operating Room: Design, Workflow, and Clinical Applications*, Oper. Neurosurg. **18**, 496 (2020).

[44] A. Elmi-Terander, G. Burström, R. Nachabé, M. Fagerlund, F. Ståhl, A. Charalampidis, E. Edström, and P. Gerdhem, *Augmented Reality Navigation with Intraoperative 3D Imaging vs Fluoroscopy-Assisted Free-Hand Surgery for Spine Fixation Surgery: A Matched-Control Study Comparing Accuracy*, Sci. Rep. **10**, 707 (2020).

[45] G. Burström, R. Nachabe, O. Persson, E. Edström, and A. Elmi Terander, *Augmented and Virtual Reality Instrument Tracking for Minimally Invasive Spine Surgery: A Feasibility and Accuracy Study*, Spine **44**, 1097 (2019).

[46] J. M. Racadio, R. Nachabe, R. Homan, R. Schierling, J. M. Racadio, and D. Babić, *Augmented Reality on a C-Arm System: A Preclinical Assessment for Percutaneous Needle Localization*, Radiology **281**, 249 (2016).

[47] *Image Guided Surgery | Image Guided System | 7D Surgical*, https://7dsurgical.com/.

[48] Z. Faraji-Dana, A. L. D. Mariampillai, B. A. Standish, V. X. D. Yang, and M. K. K. Leung, *Machine-Vision Image-Guided Surgery for Spinal and Cranial Procedures*, in *Handbook of Robotic and Image-Guided Surgery* (Elsevier, 2020), pp. 551–574.

[49] M. Sklar, P. Fatemi, H. Wadhwa, C. Leung, and C. Zygourakis, *First Case Report Using Optical Topographic-Guided Navigation in Revision Spinal Fusion for Calcified Thoracic Disk*, J. Clin. Neurosci. **91**, 80 (2021).

[50] I. H. Kalfas, *Machine Vision Navigation in Spine Surgery*, Front. Surg. **8**, 640554 (2021).

[51] *C-Arm Price Guide*, https://info.blockimaging.com/c-arm-cost-price-guide.

[52] S.-J. Hyun, K.-J. Kim, T.-A. Jahng, and H.-J. Kim, *Efficiency of Lead Aprons in Blocking Radiation − How Protective Are They?*, Heliyon **2**, e00117 (2016).

[53] M. J. Kransdorf and M. D. Murphey, *Radiologic Evaluation of Soft-Tissue Masses: A Current Perspective*, Am. J. Roentgenol. **175**, 575 (2000).

[54] R. G. Weekes, T. H. Berquist, R. A. McLeod, and W. D. Zimmer, *Magnetic Resonance Imaging of Soft-Tissue Tumors: Comparison with Computed Tomography*, Magn. Reson. Imaging **3**, 345 (1985).

[55] A. Aisen, W. Martel, E. Braunstein, K. McMillin, W. Phillips, and T. Kling, *MRI and CT Evaluation of Primary Bone and Soft-Tissue Tumors*, Am. J. Roentgenol. **146**, 749 (1986).

[56] W. R. Hogebooml, H. J. Hoekstra, E. L. Mooyaart, N. J. M. Freling, and H. S. Koops, *MRI and CT in the Preoperative Evaluation of Soft-Tissue Tumors*, Arch. Orthop. Trauma Surg. **110**, 162 (1991).

[57] H. Wu, Q. Lin, R. Yang, Y. Zhou, L. Zheng, Y. Huang, Z. Wang, Y. Lao, and J. Huang, *An Accurate Recognition of Infrared Retro-Reflective Markers in Surgical Navigation*, J. Med. Syst. **43**, 153 (2019).

[58] A. Elmi-Terander, R. Nachabe, H. Skulason, K. Pedersen, M. Söderman, J. Racadio, D. Babic, P. Gerdhem, and E. Edström, *Feasibility and Accuracy of Thoracolumbar Minimally Invasive Pedicle Screw Placement With Augmented Reality Navigation Technology*, Spine **43**, 1018 (2018).

[59] S. Garrido-Jurado, R. Muñoz-Salinas, F. J. Madrid-Cuevas, and M. J. Marín-Jiménez, *Automatic Generation and Detection of Highly Reliable Fiducial Markers under Occlusion*, Pattern Recognit. **47**, 2280 (2014).

[60] H. Sarmadi, R. Muñoz-Salinas, M. A. Berbís, and R. Medina-Carnicer, *Simultaneous Multi-View Camera Pose Estimation and Object Tracking with Square Planar Markers*, IEEE Access **7**, 22927 (2019).

[61] M. A. McDowell, C. D. Fryar, C. L. Ogden, and K. M. Flegal, *Anthropometric Reference Data for Children and Adults: United States, 2003-2006: (623932009-001)*, https://doi.org/10.1037/e623932009-001.

[62] O. Lopez-Rincon, O. Starostenko, V. Alarcon-Aquino, and J. C. Galan-Hernandez, *Binary Large Object-Based Approach for QR Code Detection in Uncontrolled Environments*, J. Electr. Comput. Eng. **2017**, 1 (2017).

[63] Z. Liao, T. Huang, R. Wang, and X. Zhou, *A Method of Image Analysis for QR Code Recognition*, in *2010 International Conference on Intelligent Computing and Integrated Systems* (IEEE, Guilin, China, 2010), pp. 250–253.

[64] T.-W. Kan, C.-H. Teng, and W.-S. Chou, *Applying QR Code in Augmented Reality Applications*, in *Proceedings of the 8th International Conference on Virtual Reality Continuum and Its Applications in Industry - VRCAI '09* (ACM Press, Yokohama, Japan, 2009), p. 253.

[65] H. Tribak and Y. Zaz, *QR Code Patterns Localization Based on Hu Invariant Moments*, Int. J. Adv. Comput. Sci. Appl. **8**, (2017).

[66] H. Zhang, C. Zhang, W. Yang, and C.-Y. Chen, *Localization and Navigation Using QR Code for Mobile Robot in Indoor Environment*, in *2015 IEEE International Conference on Robotics and Biomimetics (ROBIO)* (IEEE, Zhuhai, 2015), pp. 2501–2506.

[67] S.-J. Lee, G. Tewolde, J. Lim, and J. Kwon, *QR-Code Based Localization for Indoor Mobile Robot with Validation Using a 3D Optical Tracking Instrument*, in *2015 IEEE International Conference on Advanced Intelligent Mechatronics (AIM)* (IEEE, Busan, South Korea, 2015), pp. 965–970.

[68] M. Katanacho, W. De la Cadena, and S. Engel, *Surgical Navigation with QR Codes: Marker Detection and Pose Estimation of QR Code Markers for Surgical Navigation*, Curr. Dir. Biomed. Eng. **2**, 355 (2016).

[69] C. Kunz, V. Genten, P. Meissner, and B. Hein, *Metric-Based Evaluation of Fiducial Markers for Medical Procedures*, in *Medical Imaging 2019: Image-Guided Procedures, Robotic Interventions, and Modeling*, edited by B. Fei and C. A. Linte (SPIE, San Diego, United States, 2019), p. 97.

[70] F. Martin and R. Horaud, *Multiple-Camera Tracking of Rigid Objects*, Int. J. Robot. Res. **21**, 97 (2002).

[71] T. K. Edds Brent, *An Introduction to Operating Room Design*, https://www.dremed.com/medical_equipment_news/a-basic-guide-to-setting-up-todays-or/.

[72] *Saint Louis University Hospital Features: Operating Rooms*, https://www.ssmhealth.com/locations/saint-louis-university-hospital/slu-hospital-construction/slu-hospital-features/operating-room.

[73] X. Liu, W. Plishker, and R. Shekhar, *Hybrid Electromagnetic-ArUco Tracking of Laparoscopic Ultrasound Transducer in Laparoscopic Video*, J. Med. Imaging **8**, (2021).

[74] *Robotic Spine Surgery Program Expands at UC San Diego Health*, https://ucsdnews.ucsd.edu/pressrelease/robotic_spine_surgery_program_expands_at_uc_san_diego_health.

[75] S. G, *ArUCo-Markers-Pose-Estimation-Generation-Python* (2022).

[76] J. Gubbi, N. K. Sandeep, K. P. K. Reddy, and P. Balamuralidhar, *Robust Markers for Visual Navigation Using Reed-Solomon Codes*, in *2017 Fifteenth IAPR International Conference on Machine Vision Applications (MVA)* (IEEE, Nagoya, Japan, 2017), pp. 460–463.

[77] S. Jeon, J. Park, J. Chien, and J. Hong, *A Hybrid Method to Improve Target Registration Accuracy in Surgical Navigation*, Minim. Invasive Ther. Allied Technol. **24**, 356 (2015).

[78] J. B. West, J. M. Fitzpatrick, S. A. Toms, C. R. Maurer, and R. J. Maciunas, *Fiducial Point Placement and the Accuracy of Point-Based, Rigid Body Registration*, Neurosurgery **48**, 810 (2001).

[79] J. Rost, S. S. Harris, J. D. Stefansic, K. Sillay, and R. L. Galloway, Jr., *Comparison between Skin-Mounted Fiducials and Bone-Implanted Fiducials for Image-Guided Neurosurgery*, in edited by R. L. Galloway, Jr. (San Diego, CA, 2004), p. 766.

[80] R. Wen, W.-L. Tay, B. P. Nguyen, C.-B. Chng, and C.-K. Chui, *Hand Gesture Guided Robot-Assisted Surgery Based on a Direct Augmented Reality Interface*, Comput. Methods Programs Biomed. **116**, 68 (2014).

[81] A. Dalca, G. Danagoulian, R. Kikinis, E. Schmidt, and P. Golland, *Segmentation of Nerve Bundles and Ganglia in Spine MRI Using Particle Filters*, in *Medical Image Computing and Computer-Assisted Intervention – MICCAI 2011*, edited by G. Fichtinger, A. Martel, and T. Peters, Vol. 6893 (Springer Berlin Heidelberg, Berlin, Heidelberg, 2011), pp. 537–545.